NASA-CR-194484

GRANT
IN-18-CR
186475
76 P

(NASA-CR-194484) PRELIMINARY RESULTS: ADVANCED S-BAND STUDIES USING THE TDRSS COMMUNICATIONS SATELLITE Semiannual Report (New Mexico State Univ.) 76 p

N94-70589

Unclas

Z9/18 0186475

Preliminary Results

Advanced S-Band Studies Using the TDRSS Communications Satellite

NAG-5-2142

NASA Headquarters
Greenbelt, MD
September 15, 1993

Mr. Jeff Jenkins
Dr. William P. Osborne
New Mexico State University
Dept. of Electrical Engineering
Las Cruces, NM 88003

Table of Contents

List of Figures

List of Tables

I. Introduction

NMSU has been working under contract NAG 5-2142 to investigate the propagation channel between satellites and small user terminals on the ground. In particular, the goal of this research is to develop models for S-Band propagation based on measured data. These models may be employed in the design and development of new systems utilizing the S-Band channel. Since the last contract reporting period, NMSU has fabricated all the hardware required for the measurements, installed the equipment into the mobile platform, gone into the field on two major data collection expeditions, and obtained preliminary results from these measurements. The second data collection expedition was completed on August 11, 1993.

This semi-annual report will begin with a review of propagation models currently available to the system engineer. Secondly, the NMSU propagation study will be described. Details of the hardware and testing methodology will be presented. Finally, preliminary results will be discussed based on the data collected over the summer.

II. Current Propagation Models

This section will deal with presenting current channel models for S-Band propagation. There is, quite literally, a large volume of publications dealing with propagation and modeling of communication channels. Most of this work involves models to predict fading along line-of-sight channels, and include work on ionospheric effects and rain attenuation. The CCIR has been very active in preparing propagation model standards, and the propagation community is currently active in adding updated models and information to these standards.

Many of the CCIR models are based on categorizing every geographical region on the earth into a finite number of standard climatological zones. These zones are statistically characterized by such factors as annual rainfall, average rainfall rate, elevation, latitude, average humidity, among others. The statistics for each zone are used in most fading models.

Of more interest to the designers of Land Mobile Satellite Systems (LMSS) are propagation effects that are specific to mobile users. The most important factors that affect the mobile user are attenuation from roadside clutter (trees, buildings, bridges, etc.) and multipath from large, nearby objects. Because the cost of developing new systems is so high, companies risk their futures if systems perform poorly. This has resulted in a great deal of interest in conducting experiments resulting in accurate propagation models for mobile users. Many experiments have been conducted in recent years to measure the effects of roadside trees on communication channels, and some empirical models have been developed based on these data. Very recently, some wideband work has been done in Japan on measuring multipath in urban environments, and characterizing the coherent bandwidth of the propagation channel under some typical conditions.

Even in light of all the work that has been done to date, there are still some tremendous gaps in the current models. For example, the CCIR climate models place New Mexico in the same zone as North Carolina. While these areas may be the same in terms of annual rainfall, the seasonal nature of the rains is not accounted for. The CCIR database needs to be modified to characterize geographical areas more finely. Data is needed at more frequencies, so that frequency scaling models may be developed and refined. Many of

the experiments performed in the past were not documented as extensively as some system engineers would like, raising questions about what conditions the models really apply to. There are virtually no broadband measurements, nor data that characterizes multipath phenomena. Most work has been conducted at UHF, L-band, and K-band, where existing satellite beacons may be used for collecting data.

At the June NAPEX-XVII conference, a very recent work by Kantak, Suwitra, and Le [1] was released. Their effort has been to compile all existing propagation models into a single database. They have achieved this by using the Windows graphical user interface, and the Microsoft EXCEL spreadsheet to perform the calculations. With their software, the designer has access to 31 different propagation models, allowing the computation of Ionospheric, Tropospheric, Rain, Noise, and Empirical models for the given channel. As of this writing, the 1.0 version does not fully implement all 31 models, but an updated release should be available soon.

A number of channel models have been evolved over the years. Each model has a very specific set of conditions under which it may be applied. These models characterize different aspects of propagation. The models can be classified into the following categories: Ionospheric effects; Tropospheric effects; Rain attenuation; Roadside Shadowing; and Multipath effects. Each category will be described in detail in the sections that follow.

Ionospheric Propagation

The ionosphere is a region of the Earth's atmosphere where the radiation from the sun is sufficiently strong to form ionized particles. These ionized particles interact with these charged particles, and produce an observable effect on communications.

The first effect the plasma has is to re-orient the direction of the electric field lines in the propagating radio wave. This field rotation is know as Faraday Rotation, and can result in polarization loss in linearly polarized systems. To combat this effect, most satellite systems transmit and receive circularly polarized signals, thus eliminating the losses from Faraday rotation.

Because the material properties of the ionosphere differ from those of either air or space, the direction of propagation will change as the

radio wave passes through it. This bending effect increases as the frequency of the wave decreases. It is this bending effect that enables long distance communications on the shortwave bands (3-30 MHz). Although UHF and higher radio waves have no trouble passing through the ionosphere, the refractive effects can still produce scintillations in the received signal. In effect, some regions of the ionosphere can act as a focusing lens, and enhance the received signal strength by several decibels, while other regions behave as a diffuser and weaken the signal by several decibels. This scintillation effect is most pronounced in the tropics, where the ionospheric density is greatest. The effect is most pronounced between the hours of noon and sunset (local time), and varies significantly with latitude. Low elevation angles to the satellite also increase the amount of scintillation observed. Smith and Flock [2] presented a paper at the NAPEX XVII conference discussing the effects of the equatorial ionosphere on L-Band propagation, and presented data that showed diurnal variations on the order of 5 dB or more, depending on the elevation angle to the satellite. While this data was not collected at S-Band, a comparison of the effect at UHF Vs L-Band lead one to believe that at S-Band, scintillations are on the order of 1-1.5 dB.

Reference [2] has also presented some maps of the Earth, with zones mapped showing the intensity of the scintillation phenomena at various geographic locations. These data are based on long-term time averages, so may not be representative of instantaneous values. However, this model provides a good starting point for the system engineer in determining the type of fade margin that should be allowed for this fading phenomena.

Tropospheric Effects

The Troposphere is the bottom-most layer of the atmosphere. In the polar regions, it extends upwards to about 9 km, while in the tropics, it may extend as high as 16 km. The Troposphere contains about 90% of the mass of the earth's atmosphere, and it is here that effects such as molecular absorption take place. At S-Band, these effects are typically small. Moisture in the troposphere, discussed in the following section, plays a much larger role in propagation. Reference [1] contains models and formula for calculating propagation losses through the troposphere.

Rain Attenuation

As expected, atmospheric moisture can cause significant fades to microwave energy. The effect becomes stronger as the frequency increases from UHF to K-Band. Goldhirsh [3] has been involved in a long-term (7 year) program to collect accurate climatological data on rainfall rates in the Washington, DC area. Vogel [4] has undertaken similar measurements in about 70 other geographical areas around the Continental US. In large part, their research has focused on looking at the statistics of the rain itself; curves for the probability of the rain rate exceeding a given level in any one hour time interval have been prepared, and will likely be used to update the CCIR climatological models. Using the OLYMPUS satellite beacons at a few select sites, researchers at VPI have collected propagation data correlated with rainfall statistics to model the behavior at 12, 20 , and 30 GHz [5]. There are some frequency scaling models that may allow this latter data to be extended to S-Band.

As with the scintillation phenomena, rain attenuation increases with lower elevation angle, as the signal must pass through a longer path length of rainfall. Thus the models have strong angular dependencies built in.

In order to apply any of the rain attenuation models, information must be provided on the climate that the mobile user is in. The CCIR climate models may be used to this end. Each area is classified by annual rainfall totals, annual number of rainy days, average rainfall rate, rain height, and other climatological factors. The CCIR models provide statistics on rainfall and environmental factors that may then be included in the calculation of expected fade margins.

Roadside Tree Blockage

Vogel and Goldhirsh [6] have developed an empirical model for the effects of roadside tree blockage. From their L-Band and UHF measurements, they have developed what they call the Empirical Roadside Shadowing model (ERS). This model statistically presents cumulative distribution functions for the percent of time the channel exceeds given fade depth. Much of the data was obtained from driving route 295 in Maryland, between Washington and Baltimore. The tree cover along this route is typical of many conditions encountered in the US.

Other researchers have conducted similar studies, and have found that the ERS model fits well. The original ERS model only applies to satellite elevation angles from about 25 to 45 degrees, and tree coverage from 40% to 70% optical blockage of line-of-sight. Modifications have been made to extend elevation angle coverage to 70 degrees, and for wider variation in tree density. These modifications are referred to as the Modified Empirical Roadside Shadowing model (MERS). The original ERS model has been validated by researchers in Australia, who obtained similar fade distributions in closely matched environments.

It has been observed that trees without foliage attenuate signals much less that trees with leaves. Vogel [7] has performed measurements at UHF, L, and K bands on a particular group of trees both in the winter and in the summer. At L-band, the difference between bare and leafed was on the order of 2-3 dB, while at K band the difference was nearly 15 dB. He presents some equations that seem to allow the data to be scaled in frequency. These frequency scaling models seem to fit the data at the three frequencies well, but more frequencies need to be measured to verify the generality of the equations. Applying the scaling formula, the expected difference at S-Band is about 3-4 dB.

Several teams in the United Kingdom have undertaken similar experiments to those described above [8,9], and have included urban areas in their data collections. The type of model developed for urban areas is similar to that due to roadside trees, although its statistical behavior will be different. The data from the UK was collected at high elevation angles (60-80 degrees), since their primary interest is in satellites with Highly Elliptical Orbits, which are optimized to provide high elevation angle coverage over their service areas.

Multipath Propagation

Multipath is a condition which occurs when two or more propagation channels exists in parallel. Due to differences in path length and loss, the total received signal can vary over a wide range as the multiple channels coherently add. For example, we know that if two parallel channels exist, and differ in path length by one-half wavelength, the result is total cancellation (assuming equal amplitudes). Likewise, if the reflected signal is in phase with the direct path, the two coherently add to produce a stronger signal that either path alone.

Multipath can arise due to a number of mechanisms. As the signals propagate through the charged plasma of the ionosphere, refraction occurs. Just as we here multiple rumblings after a lightning strike as the sound waves refract through air layers, so multipath can occur with radio waves. However, at higher frequencies, this refractive effect becomes smaller, and the dominant mechanism for multipath is scattering from terrain and buildings.

The behavior of scattering from objects is strongly dependent on frequency and material properties. Materials with high conductivities, such as sheet metal siding, bodies of water, and steel-reinforced concrete, will reflect RF much better than surfaces such as dry sand or wood. "Smooth" surfaces will tend to reflect specularly (like a mirror), and can be very efficient at concentrating energy into small angular areas. "Rough" surfaces tend to reflect in a Rayleigh fashion, and scatter energy over a very broad range of angles with random phases. "Rough" and "Smooth" are relative terms, and refer to the rms surface variations with respect to the wavelength of the signal.

The transition from specular to Rayleigh scattering is gradual, as the surface changes from smooth to rough. At intermediate values, the surface can be assumed to scatter specularly, with an additional loss due to roughness. At S-Band, most natural surfaces (trees, mountains, canyons, plants, animals, etc.) are rough. It is expected that these surfaces will scatter in a Rayleigh fashion. Because the energy is spread over a wide angular range, the 1/r3 spreading loss will rapidly attenuate these multipath signals to the point where they are difficult to observe, and do not have great potential for adverse effects. Manmade structures, however, may appear quite smooth, and result in strong specular reflections. Specular reflections, being concentrated in narrow angular regions, may become even stronger than the direct path signal, if the scattering cross section of the object(s) is sufficiently large. This phenomena is very likely to be encountered in the City Canyon environment, where such large structures as skyscrapers provide locally flat, highly conductive surfaces where scattering can take place.

III. S-Band Test Methodology

The goal of the S-Band measurement program is to develop good empirical models for propagation in a variety of environments. These models should fill in the gaps in the existing S-Band propagation database. To achieve this goal, it is necessary to design an experiment that will measure channel fading and multipath phenomena over a wide bandwidth.

At S-Band, one of the few satellite resources available is the NASA Tracking and Data Relay Satellite System (TDRSS), which carries aboard each spacecraft a pair of S-Band transmitters. This resource has been made available to NMSU through special arrangements with NASA headquarters. The TDRS-Spare (hereafter referred to at TDRS-S) spacecraft is located in a geostationary orbit at 61 degrees West longitude, and is ideally placed as a signal source for propagation measurements in the continental US.

To obtain measurements over a wide bandwidth, a spread-spectrum signal is transmitted through the channel. When the signal is despread at the receiver, the symbol energy and multipath information are both measurable, and the data is effectively collected over the spread bandwidth.

The NMSU approach uplinks a Ku-band spread spectrum signal from the White Sands Ground Terminal, which is relayed back to the mobile receiver by TDRS-S at S-Band. Figure 1 illustrates the basic concept of the measurement.

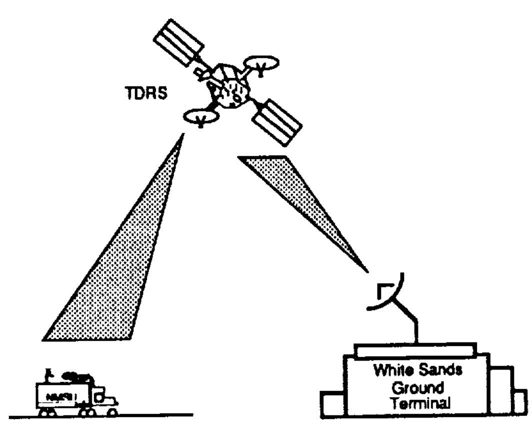

Figure 1. S-Band Test Concept

The performance of the channel is characterized by measuring the symbol energy in the received waveform. The receiver is calibrated against line-of-sight signal levels, which can be translated to absolute path loss by applying the various line-of-sight propagation models to the data.

To achieve the goal of developing accurate empirical channel models for a *variety* of environments, it is important to pick appropriate locations in which to collect the data. These locations should be representative both in elevation angle to the satellite, and in topographical features. Using the TDRS-S at 61° W, the elevation angle contours to the satellite are as shown in Figure 2 below. In this figure, all geographical locations on the 40 degree line (as an example) would observe the satellite as being 40 degrees above the local horizon. While all of the United States is not visible in the figure, it can be seen that the elevation angles vary from about 55° in southern Florida, to about 15° in the Olympic Peninsula of Washington.

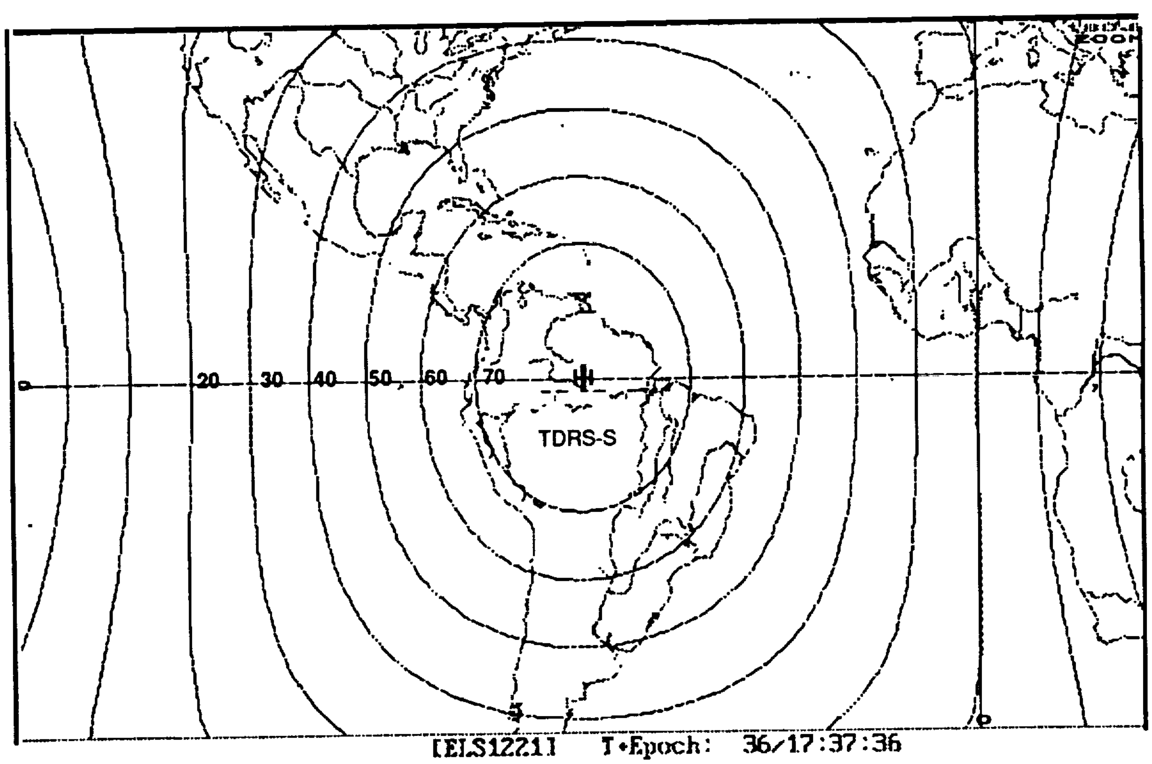

Figure 2. Look Angles to TDRS-S Satellite.

Hardware

This section will present the details of the hardware that has been developed by NMSU to conduct the channel measurements. The equipment can be broken into three main groups: Transmitter, Receiver, and Data Acquisition. The equipment van, while being a significant amount of work, is not strictly relevant to the propagation measurements. The transmitter hardware has been located at the White Sands Ground Terminal, while the receiver and data acquisition hardware are both carried in the mobile instrumentation van.

Transmitter

The transmit equipment is located at the White Sands Ground Terminal, to facilitate interfacing with the ground station equipment. The NMSU equipment consists of a PN code generator (to provide the spread spectrum signal), a data clock, and a BPSK modulator. The output of the modulator is set up to provide proper signal levels and frequencies for injection into the IF port of the ground terminal. Figure 3 below shows a block diagram of the equipment.

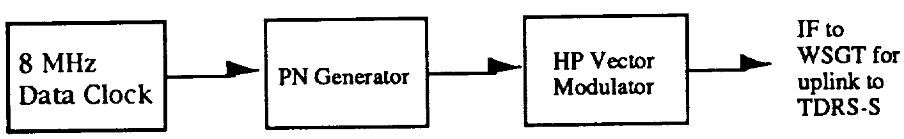

Figure 3. Transmitter Block Diagram.

The transmitted PN sequence is 1024 bits, with a chip rate of 8 MHz. The choice of sequence was limited by the availability of 1024-bit matched filters. At this chip rate, the S-Band signal occupies nearly 16 MHz of channel bandwidth.

Receiver

The NMSU S-Band receiver is a dual conversion design, incorporating a non-coherent SAW matched filter followed by an envelope detector for spread-spectrum demodulation. HP signal sources were used for local oscillators. These LO's were used to drive the mixers on an NMSU-designed and fabricated receiver chassis. Figure 4 shows a block diagram of the receiver.

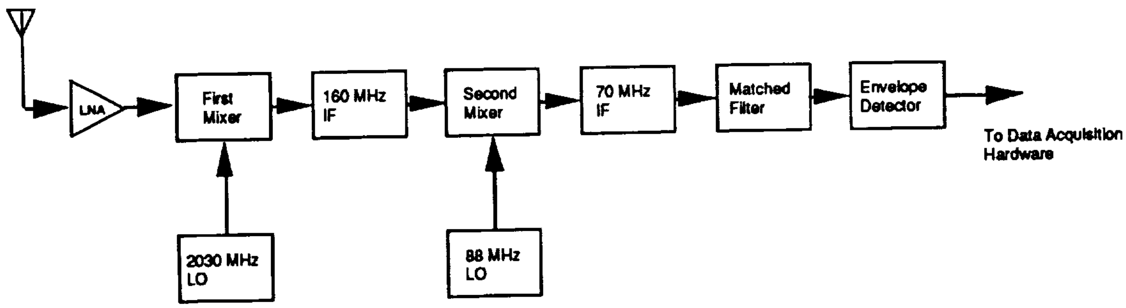

Figure 4. Block diagram of the NMSU receiver

The characteristics of the matched filter have been tailored to the PN sequence being transmitted. The output of the matched filter should look like what is shown in Figure 5. Theory says that the peak amplitude is equal to 2Es/No, where Es is the energy in each transmitted symbol, and No is the noise spectral density on the channel. This result assumes that an ideal (linear) envelope detector is used.

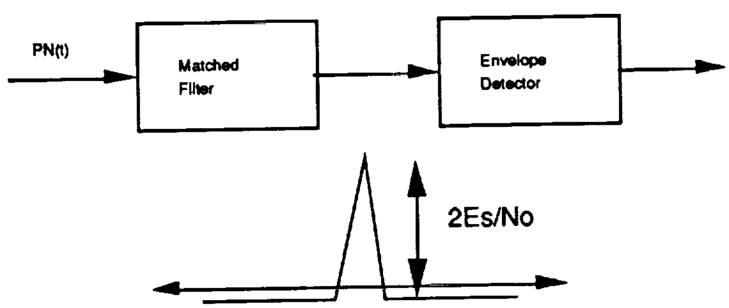

Figure 5. Matched filter response

Data Acquisition

Once the signal has been tuned, downconverted, and correlated in the matched filter, the signal waveform must be acquired and digitized. The synchronizer circuit serves to identify the data pulses in the noise, and provide uniform triggers to the waveform digitizer. NMSU has chosen to use a digitizing oscilloscope as a waveform digitizer and interface to the data storage media.

The problem of signal detection is made easier since the waveform is known. The remaining variable is the arrival time of the pulse. The inter arrival times of the pulses are known to some degree of precision, since this is determined by the transmitter clock, set to 8 MHz. The acquisition problem then becomes that of finding a pulse

of unknown amplitude, but known inter arrival times, in the midst of noise pulses of random amplitude and arrival time.

Figure 6 shows a simplified block diagram of the synchronization circuit. First, note that a simple AGC circuit it employed. The object of the experiment is to measure fading on the channel, so no AGC is present in the receiver itself. However, the tracking loop can only operate over a limited range of input signal levels. Thus, an AGC circuit within the synchronizer allows operation over the 25 dB dynamic range of the experiment.

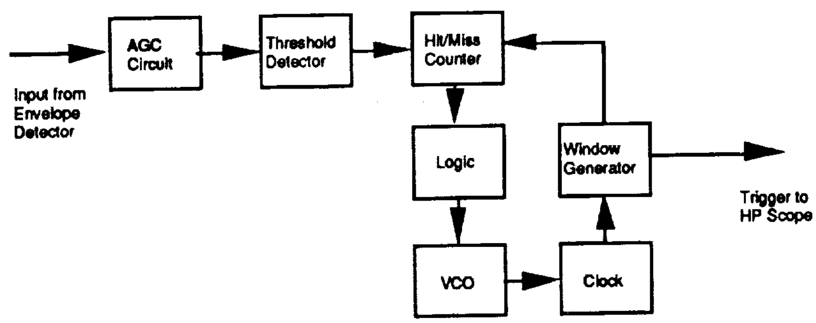

Figure 6. Block diagram of the synchronizer circuit.

After the AGC, a threshold circuit provides TTL level logic pulses whenever a pulse arrival is detected. The window generator produces narrow windows, spaced at the nominal inter arrival time of the desired signal. The logic makes a decision as to whether a pulse has arrived within the window, or outside. By keeping track of "hits" and "misses", the tracking loop attempts to keep the desired signal centered in the window. Noise pulses will not consistently fall within the window, due to the random distribution of arrivals.

Note that the synchronizer provides continuous triggers to the digitizer. This ensures that data will continue to be collected, even when the channel is severely faded. If the triggers were suppressed when an out-of-lock condition occurred, then the data would be biased. In short, if the signal were to fade for 10 seconds, we would not like to delete the "bad" data from the statistical data base. It is better to simply note that the channel is faded in excess of the dynamic range of the equipment.

Digitization and Storage

An HP digitizing oscilloscope was employed to digitize the waveforms at the envelop detector. Since the scope has a built-in computer interface via the HP-IB, it was relatively straightforward to control data collection and storage from a PC. The scope selected is an HP54505B, which can sample at rates up to 500M samples/second. The 8-bit A/D has sufficient resolution for the dynamic range of the measurement, and the 32KB of onboard RAM allowed storage of 30 waveforms of data before transfer to the host PC was necessary.

The IBM-PC which controlled the data collection was equipped with a Keithley Metrabyte HPIB card. The controlling program initialized the scope, and then began collecting data. The data was collected in bursts of 30 waveforms (which were acquired in about 200 milliseconds), and then those waveforms were transferred to the PC for writing to disk. With the transfer time between scope and PC, these 30-waveform "snapshots" were acquired every 3 seconds.

Conventional hard-disk drive technology is not capable of reliable operation under shock and vibration loads. Since the equipment is mobile while the data is being collected, it was felt that the safest way to store the data collections was to write to RAM disks, and stop the van when these RAM disks were filled. With 32M of RAM on the host PC, about 20 minutes of data can be collected before a one minute stop is necessary to write to hard disk. At the end of each days data collection, the hard disk drives were backed up onto a Colorado Memory Systems 250MB QIC-40 cartridge.

IV. Data Collection in the Field

On June 15, 1993, the data collection phase of this study began in earnest. Prior to this date, data collections had been limited to the local Las Cruces, NM area for the purpose of shaking down the system and identifying problem areas. The data collection took place over the summer in two major phases: a six week excursion through the Western US, reaching as far as the Olympic Peninsula, and a two week excursion along the Gulf Coast, reaching as far as the Mississippi-Alabama border. This section will present the details of the test routes, times, and positions that data were collected.

Western US

One of the overall goals of this S-Band study is to collect propagation in a variety of environments. Open line-of-sight areas generally are not of special interest, as the behavior of the channel is fairly well known under these ideal conditions. Therefore, NMSU sought out areas where multipath and shadowing were likely to exist. The National Parks in the Western US provide nearly ideal examples of a variety of terrain types, and have well maintained roads through these areas with slow speed limits. With this in mind, the test route was laid out to enter as many of the national parks as possible, west of the Rocky Mountains. Table I shows the areas that measurements were conducted in.

Date	Area Name	Latitude	Longitude
June 15	Albuquerque	35° 05' N	106° 38' W
June 18	Pikes Peak, CO	40° 21' N	105° 41' W
June 20	Denver, CO	39° 44' N	105° 00' W
June 24	Yellowstone NP	44° 35' N	110° 30' W
June 29	Olympic NP	47° 48' N	123° 34' W
July 2	Portland, OR	45° 31' N	122° 41' W
July 6	San Francisco	37° 47' N	122° 18' W
July 8	Yosemite NP	36° 29' N	118° 33' W
July 9	Sequoia NP	36° 29' N	118° 33' W
July 10	Mojave, CA	35° 02' N	118° 10' W
July 11	*US 54 to Vegas	37° 17' N	113° 02' W
July 12	Zion NP	37° 17' N	113° 02' W
July 13	*Flagstaff, AZ	37° 17' N	113° 02' W

* coordinates were all centered on Zion National Park

Table I. TDRS-S beam centers for Western US

Albuquerque, Denver, Portland, and San Francisco were four urban areas where data was collected. Each city provided data at different elevation angles to the TDRS-S satellite. These areas were expected to be characterized by moderate to heavy shadowing, with multipath effects from the buildings. Pikes Peak, Yellowstone, Olympic, and Sequoia were expected to provide moderate to heavy tree blockage with and without mountains. Yosemite and Zion parks were expected to provide sheer rock walls and natural multipath environments, with moderate to complete blockage of the direct path signal. The actual results from these measurements will be discussed later. In all, about 42 hours worth of data were gathered in and around the areas indicated above.

Gulf Coast and Plains

The data collections in the Western US provided data in canyons, deserts, and mountains. However, there were two shortcoming with this data. First, the elevation angles to the TDRS-S satellite at 61W were all quite low - from 13 to 29 degrees. Secondly, nearly all the tree cover was coniferous. By planning a second excursion along the Gulf Coast, urban areas such as Houston could be tested. With the substantially higher elevation angle to the satellite (nearly 45 degrees), differences in multipath propagation could potentially be observed. The return path through Mississippi, Arkansas, and Missouri would likewise provide data on light to moderate shadowing from hardwoods such as Oak, Birch, Maple, Cottonwood, and others.

With these goals in mind, and removing all the excess set-up days from the schedule, a second trip was planned. In addition to collecting data in specific locations such as Houston and the Ozarks, as much data as possible was collected under *normal* driving conditions in these areas. In the Western US trip, areas were sought out where peculiar propagation phenomena might be observed. In contrast, this second trip was intended to collect data under typical conditions an end user might find themselves in driving to and from work, or along interstate and two lane highways. Table II below shows the locations of the TDRS-S beam center for the duration of the trip. In all, about 27 hours of propagation data was collected along 9 portions of the route. One day worth of data collection was missed due to mechanical problems in the field.

Date	Location	Latitude	Longitude
8/2/93	Salt Flat, TX	31° 44' N	105° 05' W
8/3/93	Rock Springs, TX	30° 00' N	100° 12' W
8/4/93	Schulenburg, TX	29° 40' N	96° 54' W
8/5/93	Lake Charles, LA	30° 12' N	93° 10' W
8/6/93	Hattiesburg, MS	31° 19' N	89° 16' W
8/7/93	Greenville, MS	33° 27' N	90° 37' W
8/8/93	Clinton, AR	35° 36' N	92° 27' W
8/9/93	Westville, OK	35° 59' N	94° 34' W
8/10/93	Elk City, OK	35° 25' N	99° 21' W
8/11/93	Roswell, NM	33° 23' N	104° 30' W

Table II. TDRS-S beam centers for Southeastern US

V. Data Reduction & Preliminary Results

The raw data collected in the field consisted of digitized waveforms at the output of the matched filter. The data needed to be processed through computerized algorithms to reduce the data to humanly manageable proportions. NMSU has developed an integrated software package that automatically processes the raw data tapes, and outputs files containing the amplitude and time of the correlation peaks. The operations performed by this package follow:

Step 1: The HP84505B digitizing scope incorporates an 8-bit A/D convertor. However, the data is transferred over the HPIB by the firmware as a 16 bit integer. Once stored by the host computer, the samples must be converted back into voltages for processing.\

Step 2: The HP84505B has a limited amount of internal RAM. When this storage is filled with waveform samples, the data collection must stop momentarily to transfer the samples to the host computer. The on-board RAM is sufficient to store 30 waveforms. The 30 waveforms in each group are collected in rapid succession. In all, it takes about 200 milliseconds to collect each group of waves, and nearly 3 seconds to transfer the data to the host computer. This results in data being collected in bursts along the route, with about 3 seconds between each burst. When faced with the need to perform some waveform averaging to accurately locate the correlation peaks in the noise, the natural choice was to average each group of 30, providing a "snap shot" of the channel once each 3 seconds.

Step 3: Once the waveforms have been restored to voltage and averaged, the correlation peak from the matched filter is located and recorded. The value of this peak is directly related to the signal-to-noise ratio on the channel.

Step 4: The propagation data must be calibrated. In the S-Band data processing, the average value of signal strength along the line-of-sight path is used to reference all the fading statistics. Line-of-Sight data is collected at the beginning and end of each data collection, and the data reduction software applies this calibration to all the propagation measurements.

Step 5: A final correction to the data is made to account for the envelope detector response. The magnitude of these corrections was determined by measuring the envelope detector response at known

signal-to-noise ratios. Upon completion of this step, the signal strength versus time data is available for statistical analysis.

Step 6: The cumulative fade distributions are computed from the time-amplitude response of the channel.

This first-cut data reduction has been accomplished on the data. In this initial cut, it has been assumed that the terrain remained very similar throughout each day's data collection. This allows statistics to be accumulated on each data set, without subdividing each set of data. In the real world, it is difficult to drive a 200 mile route and maintain uniform tree cover or similar terrain throughout. The result is that each day's data collection contains some elements from different types of terrain.

The time-amplitude plots and the associated Cumulative Distribution of Fade (CDF) plots can be located in Appendix A. Upon inspection, these curves can be grouped into three categories, according to the link margin required to maintain communications 95% of the time. Figure 7 shows the CDF's for these groups, obtained by accumulating statistics on all of the data collected. The discussion below will be referring back to the curves in figure 7.

Type I fading

Many of the areas in which data collections were made had few roadside obstacles to block the signal or induce multipath conditions. The roads that traveled through these areas permitted line-of-sight communications, with fades occurring only when passing under bridges, or passing through road cuts. In particular, driving through the Mojave Desert, or along routes in Arizona, Nevada, and New Mexico, few features were found to degrade the communications channel.

Other areas in which data was gathered had significant tree cover, but due to well-kept roads, the branches did not hang overhead. When the elevation angle to the satellite is relatively high (35 to 45 degrees), these roadside trees did not seriously degrade the channel performance.

Type I fading is characterized by infrequent fades. When fades occur, they are typically deep, but not always. The NMSU data

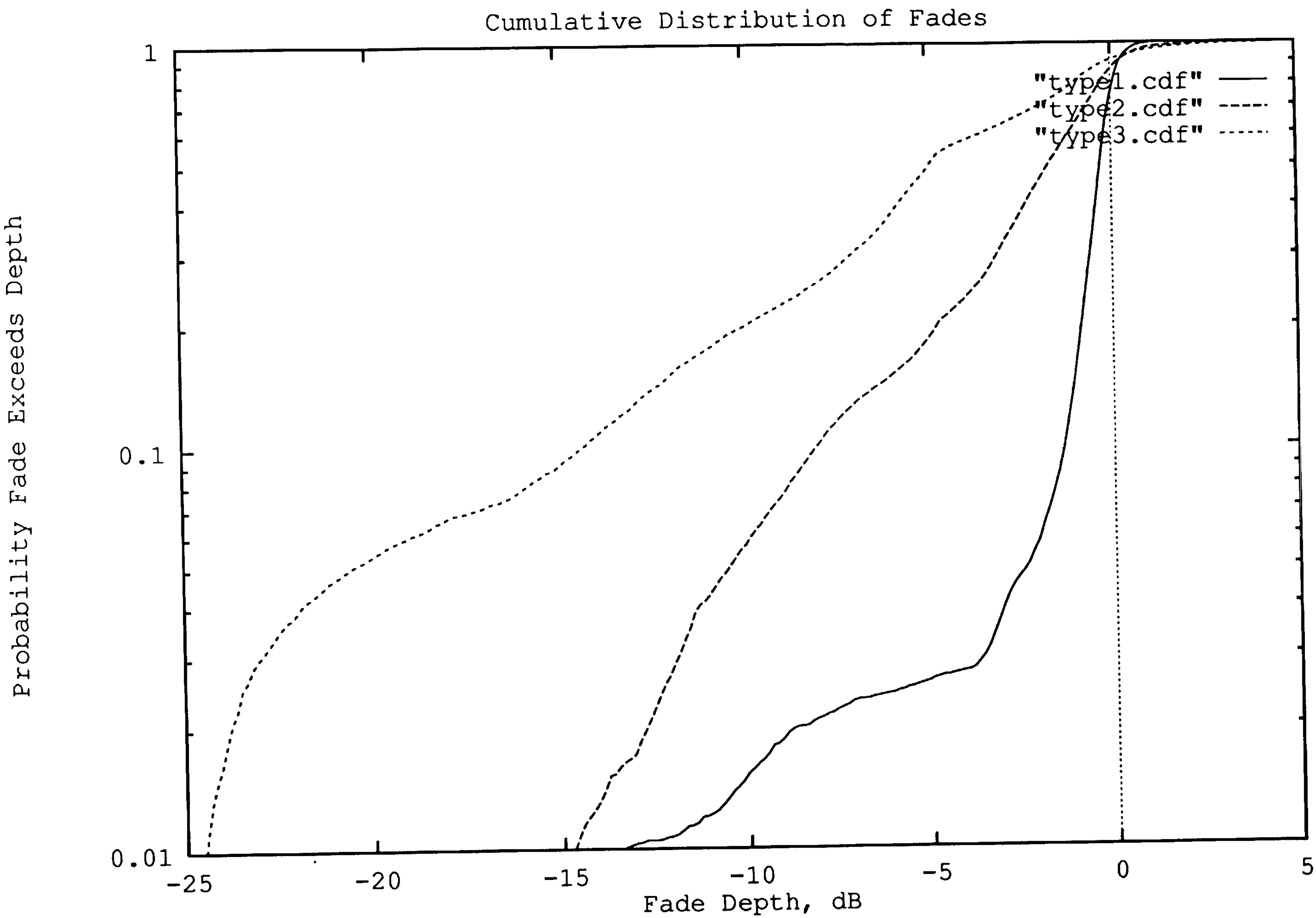

Cumulative Distribution of Fades
Probability Fade Exceeds Depth
1
0.1
0.01
-25
-20
-15
-10
-5
0
5
Fade Depth, dB
"type1.cdf"
"type2.cdf"
"type3.cdf"

indicate that a 3 dB link margin will allow access to the link in excess of 95% of the time.

Type II fading

When the elevation angle to the satellite becomes low (less than 25 degrees), more frequent fading is observed on the channel. Low hills and road cuts are much more likely to obstruct the line-of-sight to the satellite, and roadside trees begin to have a larger effect. Figure 8 shows the geometry of the roadside trees, and how this shadowing effect increases as the elevation angle decreases. Even at higher elevation angles, overhanging foliage will cause fading on the channel. Most of the areas along the gulf coast exhibited Type II fading, believed to be mainly caused by the roadside trees. Some light urban areas also exhibit Type II fading.

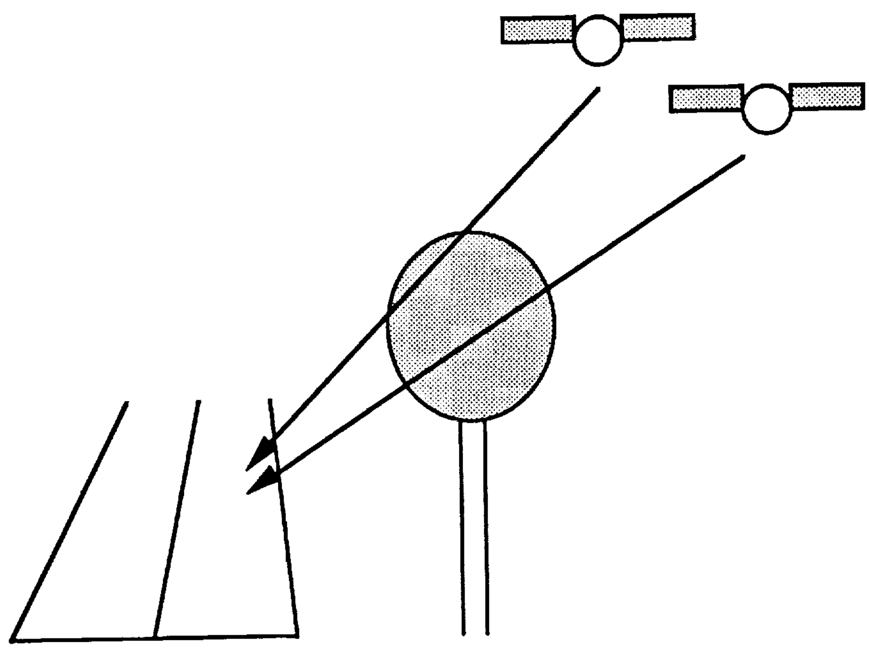

Figure 8. Roadside Tree Geometry

The Type II curves are characterized by frequent deep fades, with periods of line-of-sight propagation in between. The data gathered by NMSU indicate that for 95% link availability, a 10 dB link margin is required.

Type II conditions are similar to the conditions under which Vogel and Goldhirsh developed their Empirical Roadside Shadowing (ERS)

model for L-Band propagation [a]. The ERS model characterizes the density of the roadside trees in terms of a parameter called Percentage of Optical Blockage. This was measured by the researchers by using the light meter in a 35mm camera (which was pointed in the general direction of the helicopter they used as a signal source). Since NMSU did not measure this quantity, it is impossible to precisely compare the L-Band data with the S-Band results. However, the ERS model does predict a log-linear characteristic, with a slope similar to that seen in the Type II curve. Figure 9 shows the ERS prediction for a 35 degree elevation angles along with the average Type II fading response. It is believed that the fading at S-Band was less due to lighter roadside tree coverage; however, this figure does show some of the similarities between the emerging S-Band fading statistics and the L-Band ERS model.

Type III fading

Under extreme conditions, the communications channel may not be available with reasonable link margins. Low elevation angles, dense tree cover, deep canyons, and city canyons provide the worst possible conditions for mobile satellite communications. NMSU went out into the Western US for six weeks during the summer, and looked for such areas to gather propagation data in. Not only were the environments harsh, but low elevation angles to the satellite made the situation worse. Olympic and Sequoia parks had extreme tree cover, with the roads passing under the foliage. Yosemite and Zion parks had deep canyons where the line-of-sight was completely obstructed. Denver, Portland, and San Francisco had many areas where the line-of-sight was blocked.

Type III conditions are characterized by nearly continuous fading conditions. The data obtained by NMSU under Type III fading conditions show that fade margins of 20 dB are necessary to provide a link availability of 95%.

Urban Areas

The urban environments measured during the S-Band study have exhibited frequent and deep fading. Denver, Portland, and San Francisco all fit into the Type III fading channel category. As discussed in the section on multipath propagation, it is expected that much of the fading in the urban environment is due to multipath. More will be learned when the data is processed for this phenomena.

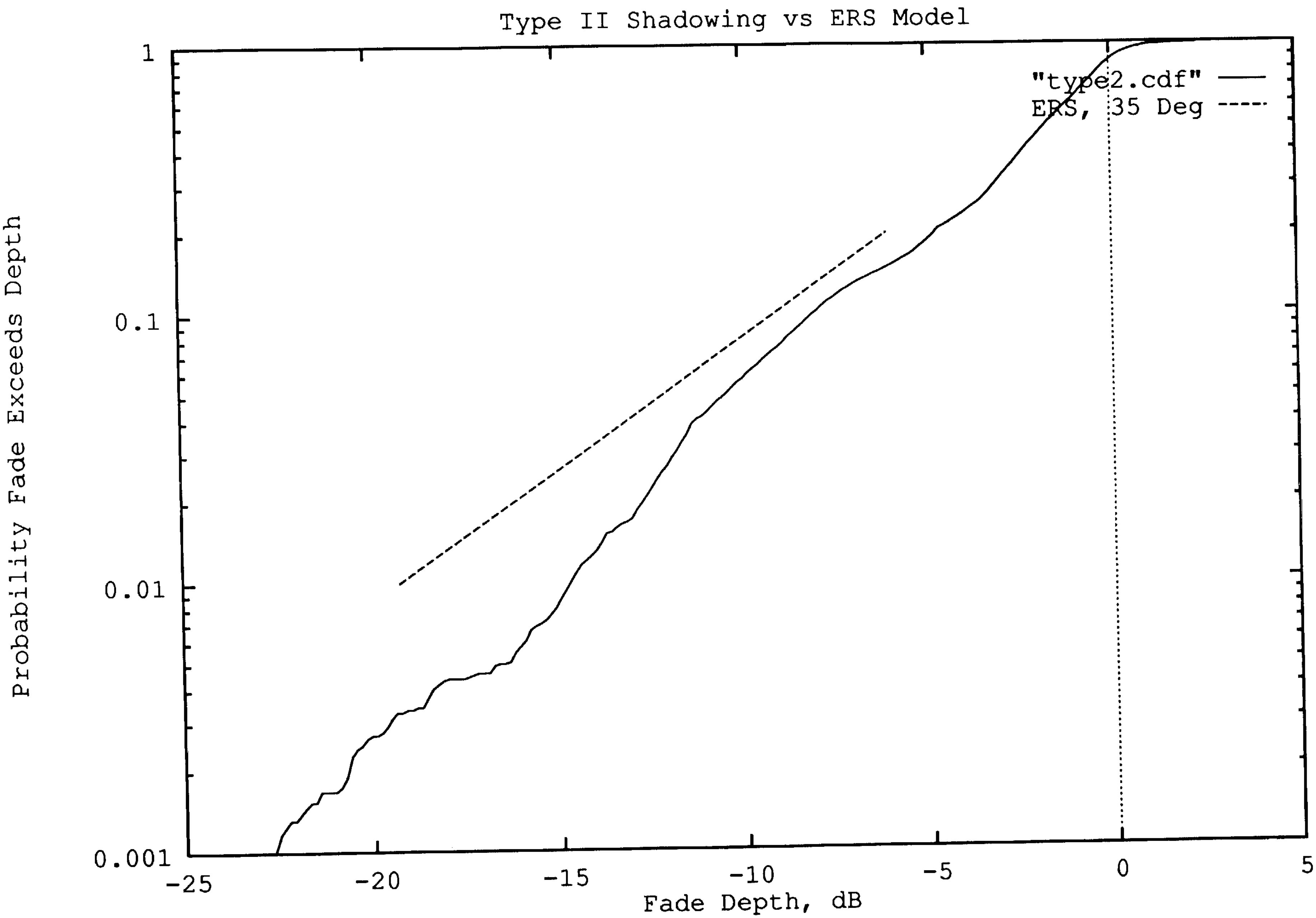
Type II Shadowing vs ERS Model
Probability Fade Exceeds Depth
1
0.1
0.01
0.001
-25
-20
-15
-10
-5
0
5
Fade Depth, dB
"type2.cdf"
ERS, 35 Deg

However, it can be said that in terms of fade distribution, the city canyon behaves much like heavy tree cover. Figure 10 shows the fade distributions for four of the urban areas tested. It should be kept in mind that the data collected in these areas is a mixture of interstate highways approaching the areas, the suburban areas, and the city canyon areas. The video tapes of the route must be examined so that the true city-canyon data may be processed separate from the suburban areas.

One thing that is evident from this first pass data reduction is that the urban area generally has frequent and deep fading on the channel. More urban data is needed to draw any clear conclusions about angular dependence of this fading.

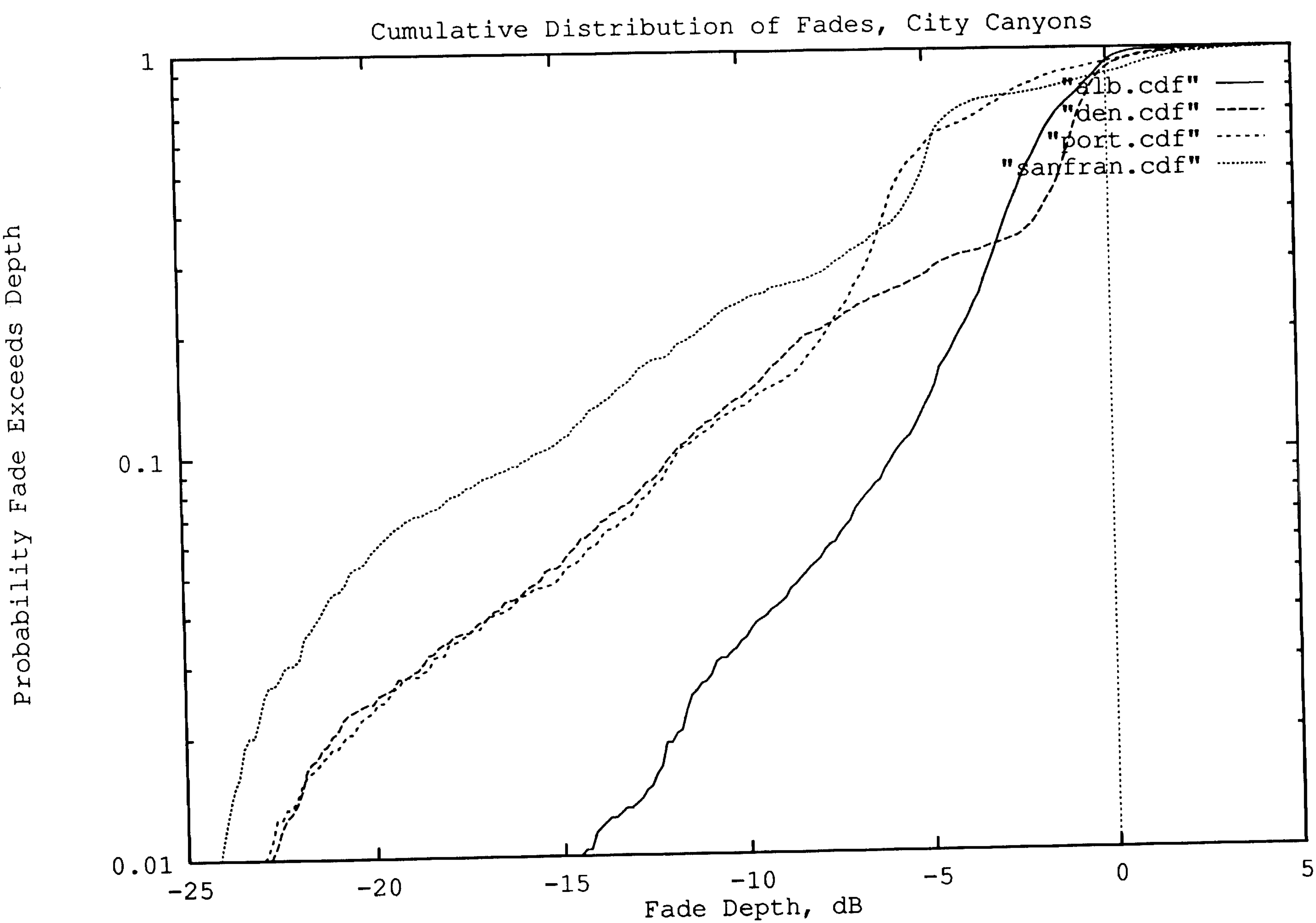

Cumulative Distribution of Fades, City Canyons
Probability Fade Exceeds Depth
1
0.1
0.01
-25
-20
-15
-10
-5
0
5
Fade Depth, dB
"alb.cdf"
"den.cdf"
"port.cdf"
"sanfran.cdf"

VI. Summary and Conclusions

As of this report, the propagation data collected in New Mexico, the Western US, and the Southeastern US has been reduced to first order. Fade-Time plots have been prepared on the individual data collections, and initial fade distribution statistics computed. The data collections can be grouped into three fading-channel classes, identified as Type I, II, and III. The Type I channel is most nearly the same as the line-of-sight channel, while the Type III channel is characterized by nearly continuous deep fades. The Type II channel is believed to be an overall average condition for mobile users, and exhibits fade distributions with similar characteristics to the Empirical Roadside Shadowing model currently in use for L-Band mobile systems. Table III summarizes the fade margins necessary for the various propagation channels.

Channel Type	Median Fade Level	Margin Required for 95% link availability
Type I	1 dB	3 dB
Type II	3 dB	10 dB
Type III	6 dB	20 dB

Table III. Fade margins required for channel types.

References

[1] Kantal, A. , K. Suwitra, and C. Le, "Database Software for Propagation Models", JPL Publication JPL D-10861, June 1993.

[2] Smith, E.K. and W. Flock, "Effects of the Equatorial Ionosphere on L-Band Earth-Space Transmissions", Presented at the NAPEX-XVII conference, Pasadena, CA June 15, 1993

[3] Goldhirsh, J, "Rain rate duration statistics derived from the mid-atlantic coast rain gauge network", presented at the NAPEX-XVII conference, Pasadena CA June 1993.

[4] Vogel, W., "Long duration measurements of scintillation and fading on a low elevation angle, 11 GHz satellite path", presented at the NAPEX-XVII conference, Pasadena, CA June 1993.

[5] Pratt, T. and F. Haidra, "Results from a study of scintillation behavior at 12, 20, and 30 GHz using the Virginia Tech OLYMPUS receivers", presented at NAPEX-XVII

[6] Goldhirsh, J and W. Vogel, "Mobile satellite system fade statistics for shadowing and multipath from roadside trees at UHF and L-Band", *IEEE Trans. Antennas Propagat*, vol AP-37, no. 4, pp. 489-498, April 1989

[7] Vogel, W. and J. Goldhirsh, "Tree attenuation at 20 GHz: foliage effects", presented at the NAPEX-XVII conference, Pasadena, CA June 1993

[8] Evans, B., "Narrowband channel measurement results at L- S- and KU-Bands and plans for wideband measurements", presented at the NAPEX-XVII conference, Pasadena, CA June 1993

[9] Smith, H., J.G. Gardiner, and S.K. Barton, "Measurements of the satellite-mobile channel at L & S Bands", Proceedings of the Third International Mobile Satellite Conference, pages 319-324.

Appendix A
Propagation Data at S-Band

This Appendix presents the individual data curves from the S-Band study. They have been grouped into three categories, according to the type of fading distribution in each area. The plots begin with those areas having the mildest degree of fading, and progress to those areas with moderate and finally severe fading. The following comments pertain to some of the data collections.

Type I Curves

Oklahoma

This data was collected along I-40, from just west of Oklahoma City, to the Texas border. The few momentary fades are most likely due to driving under occasional bridges across the interstate highway.

Anthony, NM

This set of data was collected along I-10. The route began at the Texas-New Mexico border, and proceeded through El Paso, TX. The route ended near Kent, TX. Some fades were noted as the equipment went through the urban areas of El Paso. Note the one particularly long fade that occurred about 1/4 of the way into the run. This fade introduced a discontinuity into the distribution function. The video tapes will be analyzed to identify the cause of this fade.

New Mexico

This route began near Elkins, NM (about 50 miles west of Roswell) and proceeded to the White Sands national monument. The run began in a very open and clear area. Each of the three areas where fading is evident are likely due to passing through cities. The times are consistent with passage through Tularosa, Alamogordo, and Holloman AFB. The video will have to be analyzed to identify the exact source of the observed fading.

US 180

This test began along US 180 in Arizona. The road was two-lane. For the first two hours, the terrain was open and clear, with a few

scattered trees, roadcuts, and distant mountains. As the route crossed into New Mexico, the road began to enter the mountains. The route gradually entered denser tree cover, which by the end of the run was dense enough to make calibration difficult.

Mojave, CA

This data was collected along a two-lane highway through the Mojave Desert. The entire route was clear and open. The only notable exceptions were a few shallow road cuts through low hills.

Pikes Peak

The route was driven in the vicinity of Pikes Peak. The road had many twists and turns, and light tree cover. Line-of-sight conditions were found in many places along the route, as were medium to heavy shadowing conditions from trees.

Type II Curves

Katy, TX to Galveston, TX

This data is characterized by frequent deep fades, but line-of-sight levels can be seen between the fades.

Marshall, AR to Springdale, AR

There were many roadside trees along this route.

Albuquerque, NM

The first 20 minutes was in a very light urban area. Then the truck moved closer towards the heart of the city. Once the receiver was moved into the "city canyon", the deepest and most frequent fades are observed. Towards the end of the data collection, the truck was back into a light urban area.

Type III Curves

Olympic National Park

The tree cover was so dense that it was difficult to find a clear line-of-sight for calibration. There were extended periods of time where

the signal was at or below the dynamic range of the apparatus. These deep fades were caused not only by the density of the tree cover, but also by the low elevation angle to the satellite (17 degrees). Note that even under these adverse conditions, there were many holes in the canopy where the signal could be received.

Yosemite National Park

The terrain around Yosemite National Park can best be described as mountainous, with moderate tree cover. The mountains were situated such that line-of-sight was frequently blocked. The route proceeded down into the canyon. The route then proceeded out of the canyon along the northern rim. Two locations are discernible where the channel was relatively unfaded. The first, about mid-run, was along the rim in a clearing. The second area was along the road out of the canyon, near the calibration site.

Sequoia National Park

Data collection began about an hours drive away from the giant redwoods. The boundary of the forest is rather abrupt, and coincides with the noticeable change in character of the channel about 1/3 of the way into the run. The park roads are not representative of roads in other forests, as a deliberate effort has been made to bring the road to the trees. The canopy extended completely overhead. Right at the end of the data collection, as the road wound down a switchback out of the park, a clear line-of-sight was found. This was used as the post calibration site.

Denver

This data was all taken in the urban areas of Denver. The suburban areas at the beginning and end of the run seem a little better than the city canyon in the middle of the run.

Portland

Between the heavy urban areas, tree cover, and low elevation angle to the satellite, the conditions were pretty adverse.

San Francisco

City canyon at its worse. Low angles and tall buildings caused nearly continuous deep fading. One region in the middle of the run looks flat and clear. However, the time coincides with a 5 minute stop the driver made in the middle of the data collection. The parking lot was relatively open. This stop has introduced some bias into the measurements, and will be removed in later data processing.

Type I Shadowing

Oklahoma

Anthony, NM to Kent, TX

Elkins, NM to White Sands

US 180 in Arizona

Mojave Desert, CA

Vicksburg, MS

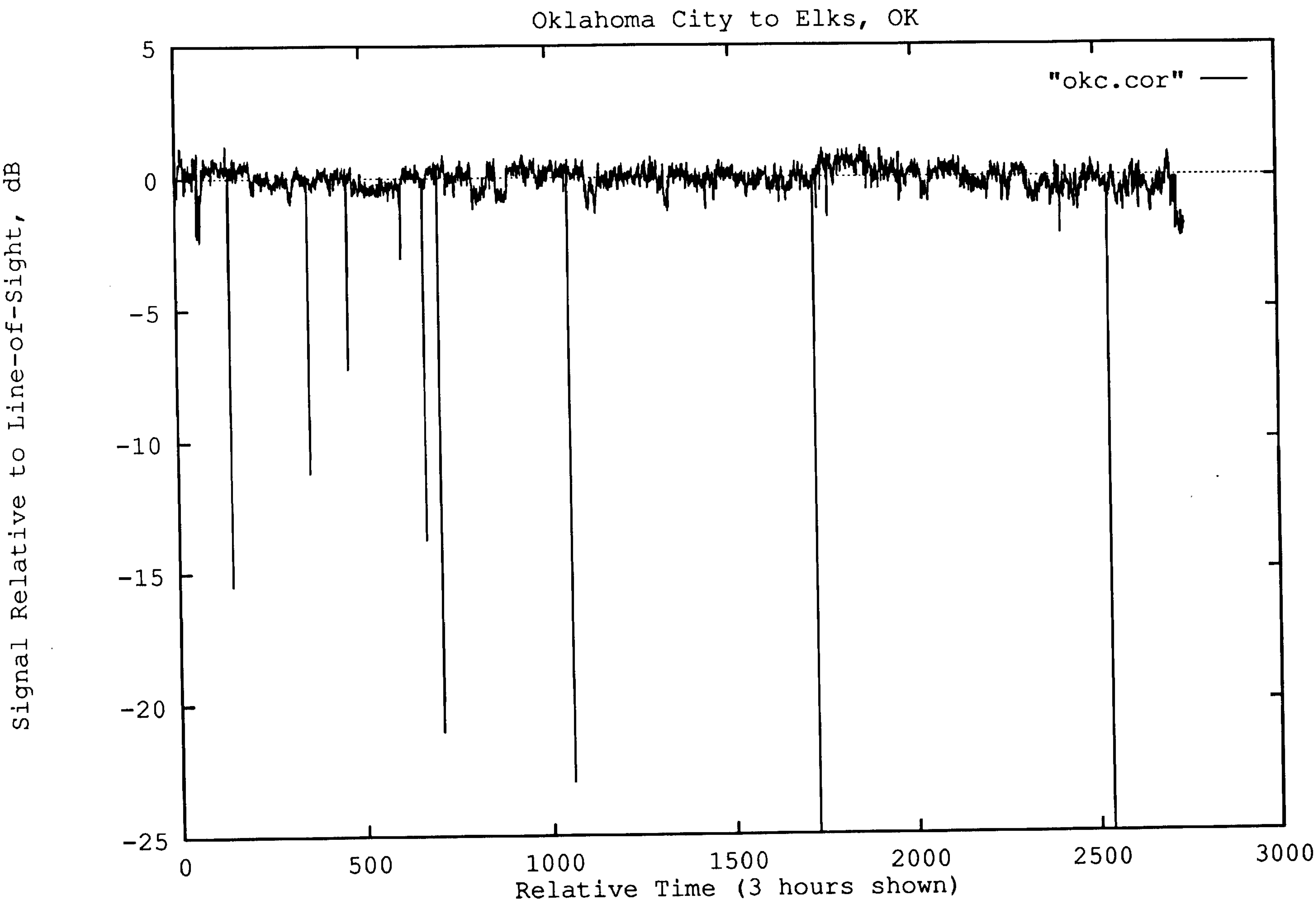

Oklahoma City to Elks, OK
"okc.cor"
Signal Relative to Line-of-Sight, dB
5
0
-5
-10
-15
-20
-25
0
500
1000
1500
2000
2500
3000
Relative Time (3 hours shown)

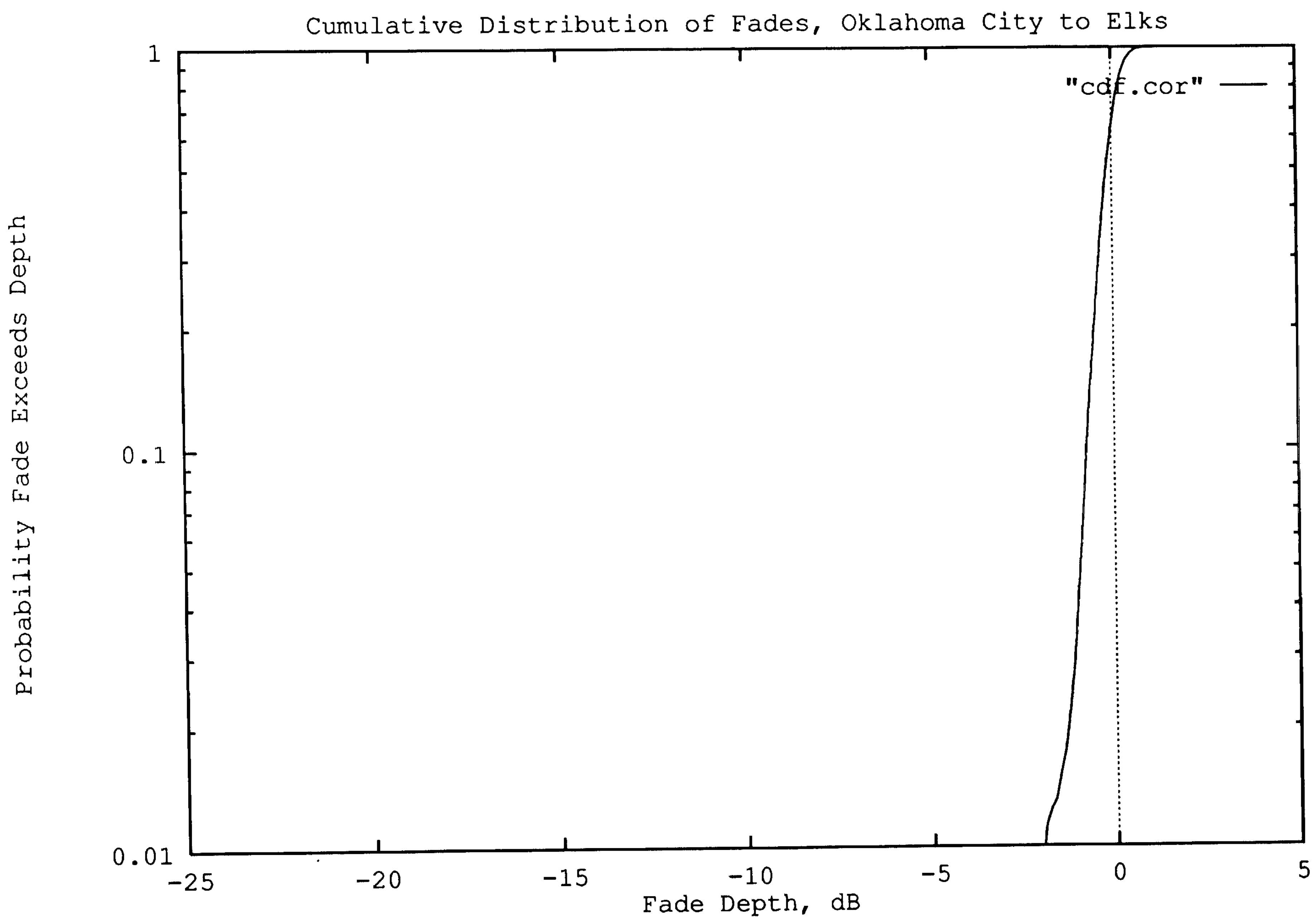

Cumulative Distribution of Fades, Oklahoma City to Elks
"cdf.cor"
Probability Fade Exceeds Depth
1
0.1
0.01
-25
-20
-15
-10
-5
0
5
Fade Depth, dB

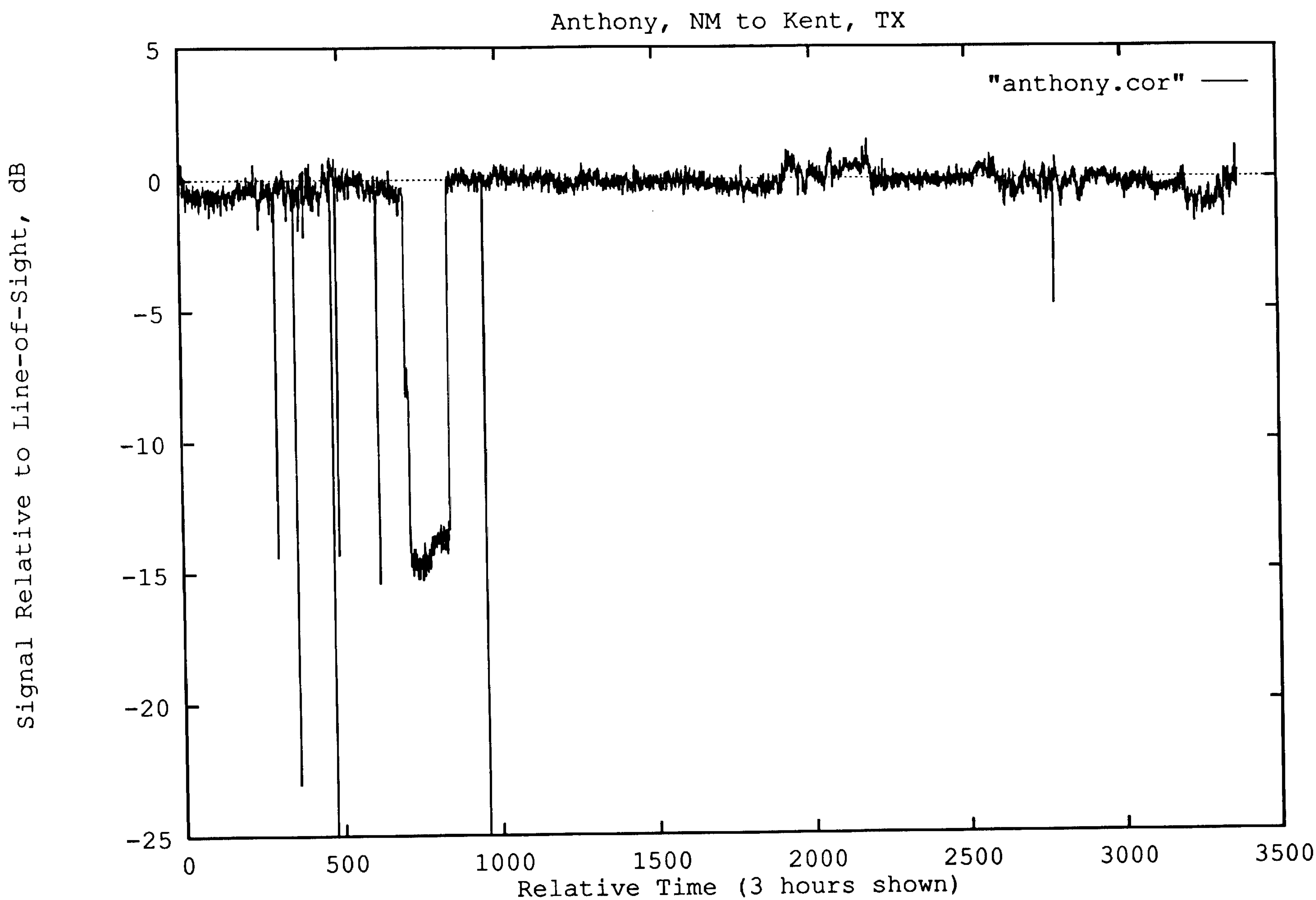
Anthony, NM to Kent, TX
"anthony.cor"
Signal Relative to Line-of-Sight, dB
5
0
-5
-10
-15
-20
-25
0
500
1000
1500
2000
2500
3000
3500
Relative Time (3 hours shown)

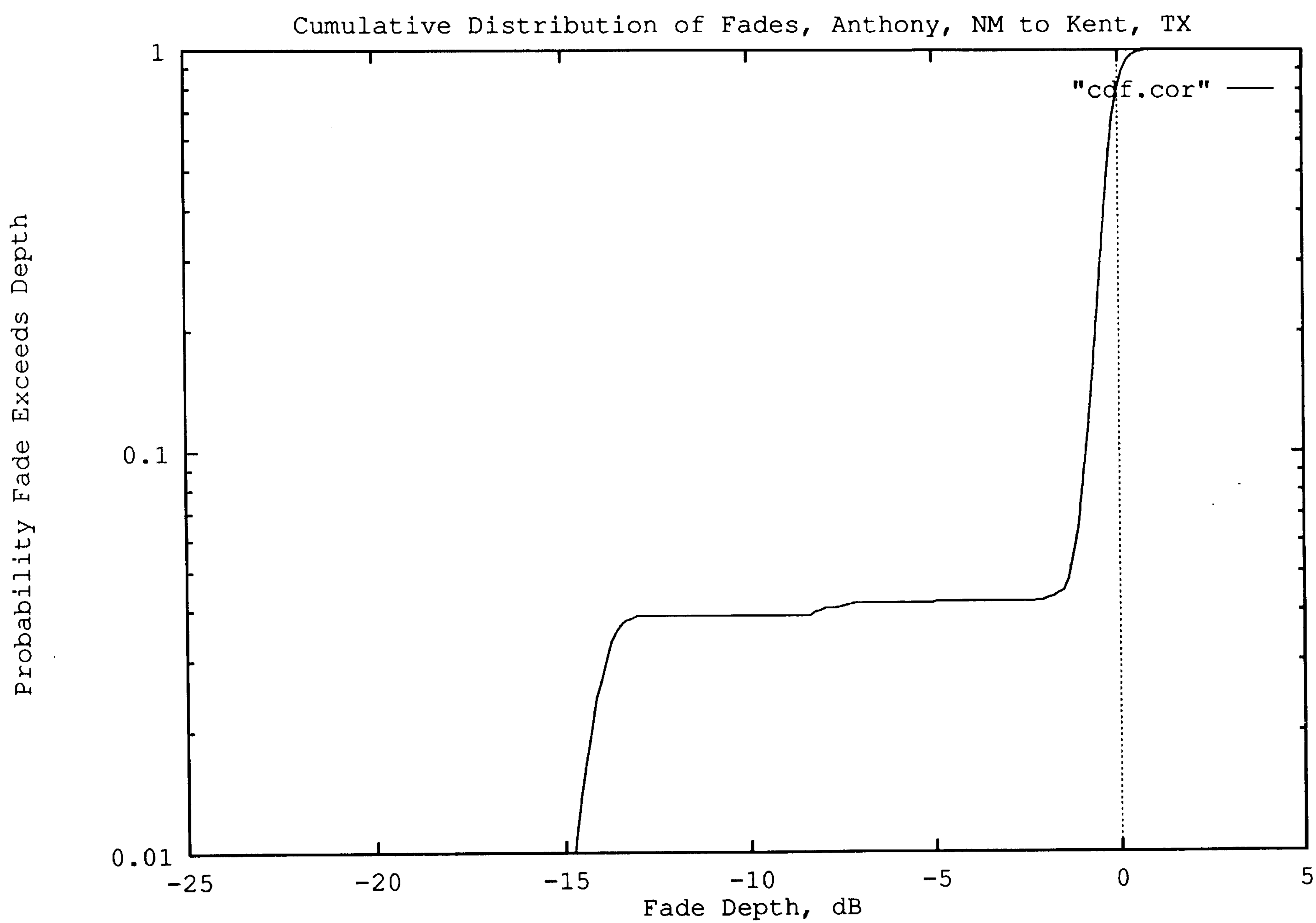
Cumulative Distribution of Fades, Anthony, NM to Kent, TX
"cdf.cor"
Probability Fade Exceeds Depth
1
0.1
0.01
-25
-20
-15
-10
-5
0
5
Fade Depth, dB

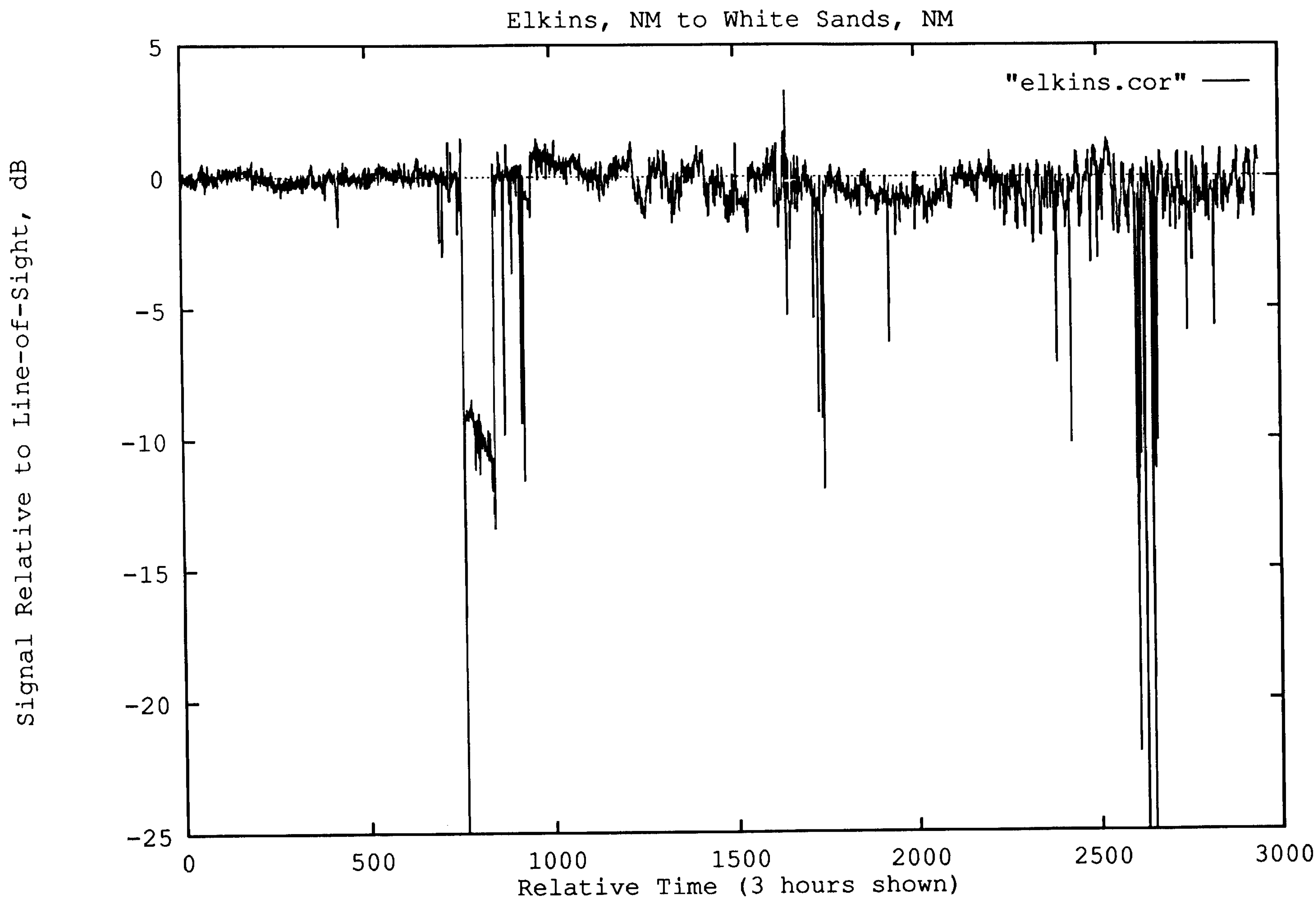
Elkins, NM to White Sands, NM
"elkins.cor"
Signal Relative to Line-of-Sight, dB
5
0
-5
-10
-15
-20
-25
0
500
1000
1500
2000
2500
3000
Relative Time (3 hours shown)

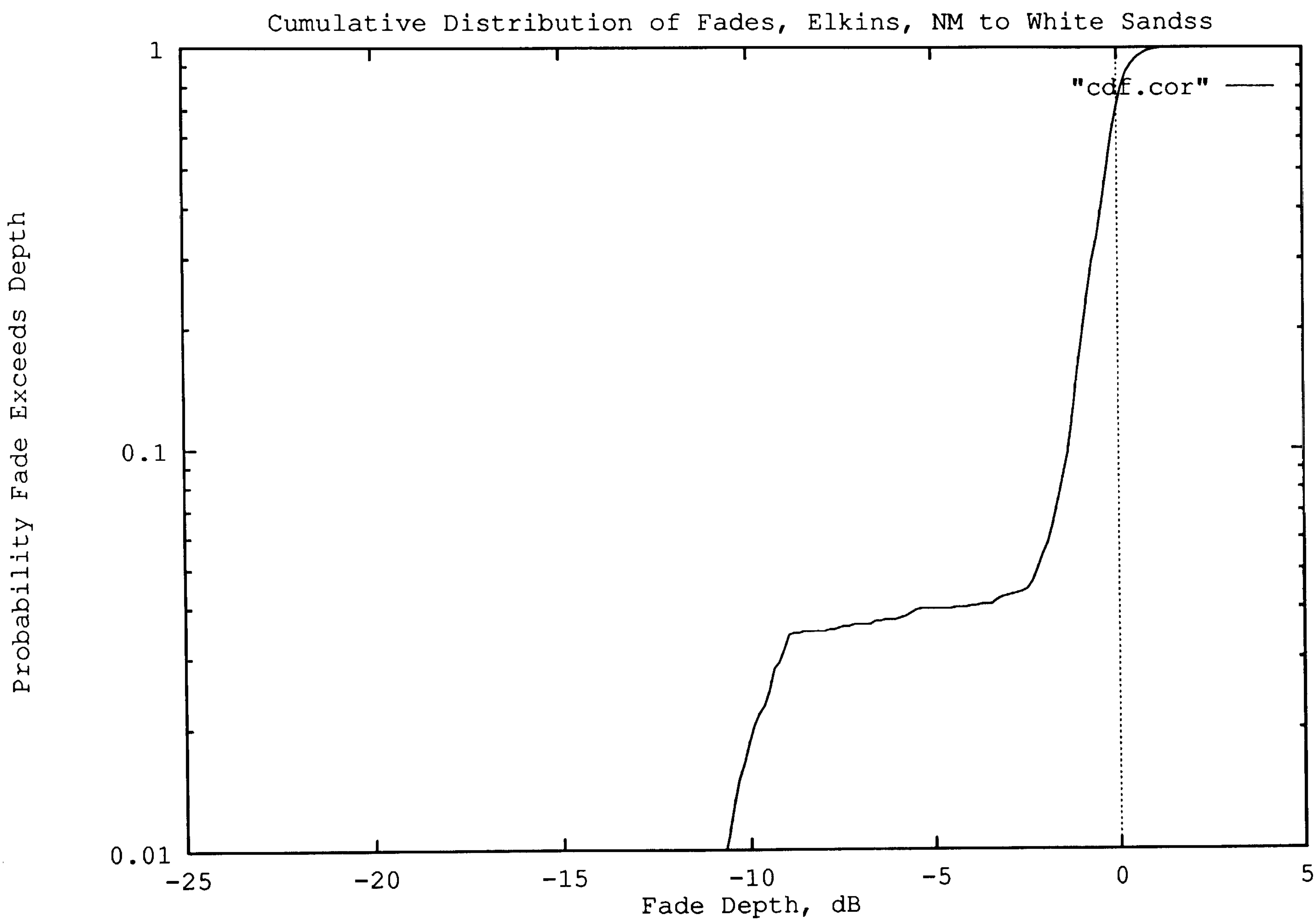
Cumulative Distribution of Fades, Elkins, NM to White Sandss
"cdf.cor"
Probability Fade Exceeds Depth
1
0.1
0.01
-25
-20
-15
-10
-5
0
5
Fade Depth, dB

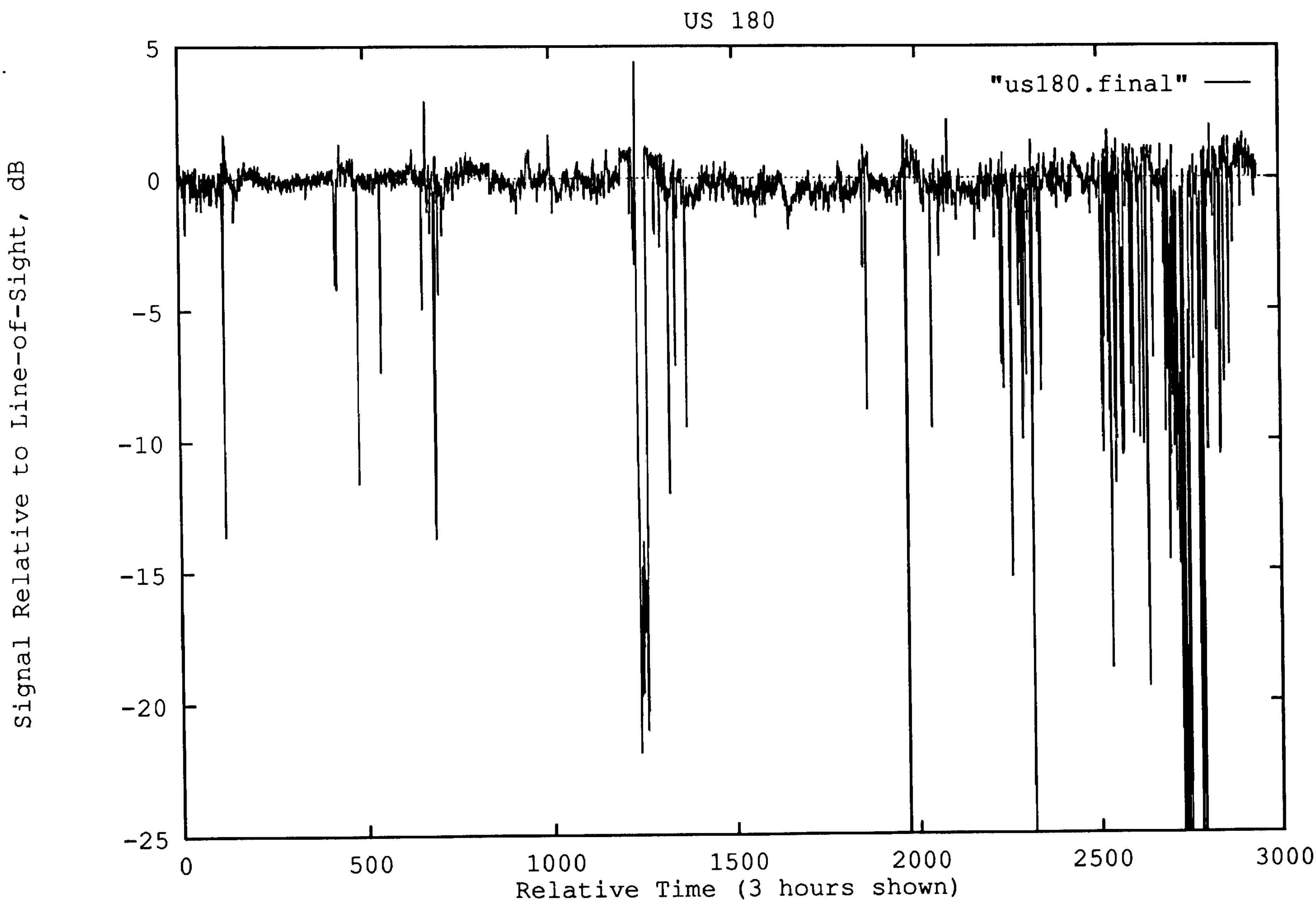

US 180
"us180.final"
Signal Relative to Line-of-Sight, dB
5
0
-5
-10
-15
-20
-25
0
500
1000
1500
2000
2500
3000
Relative Time (3 hours shown)

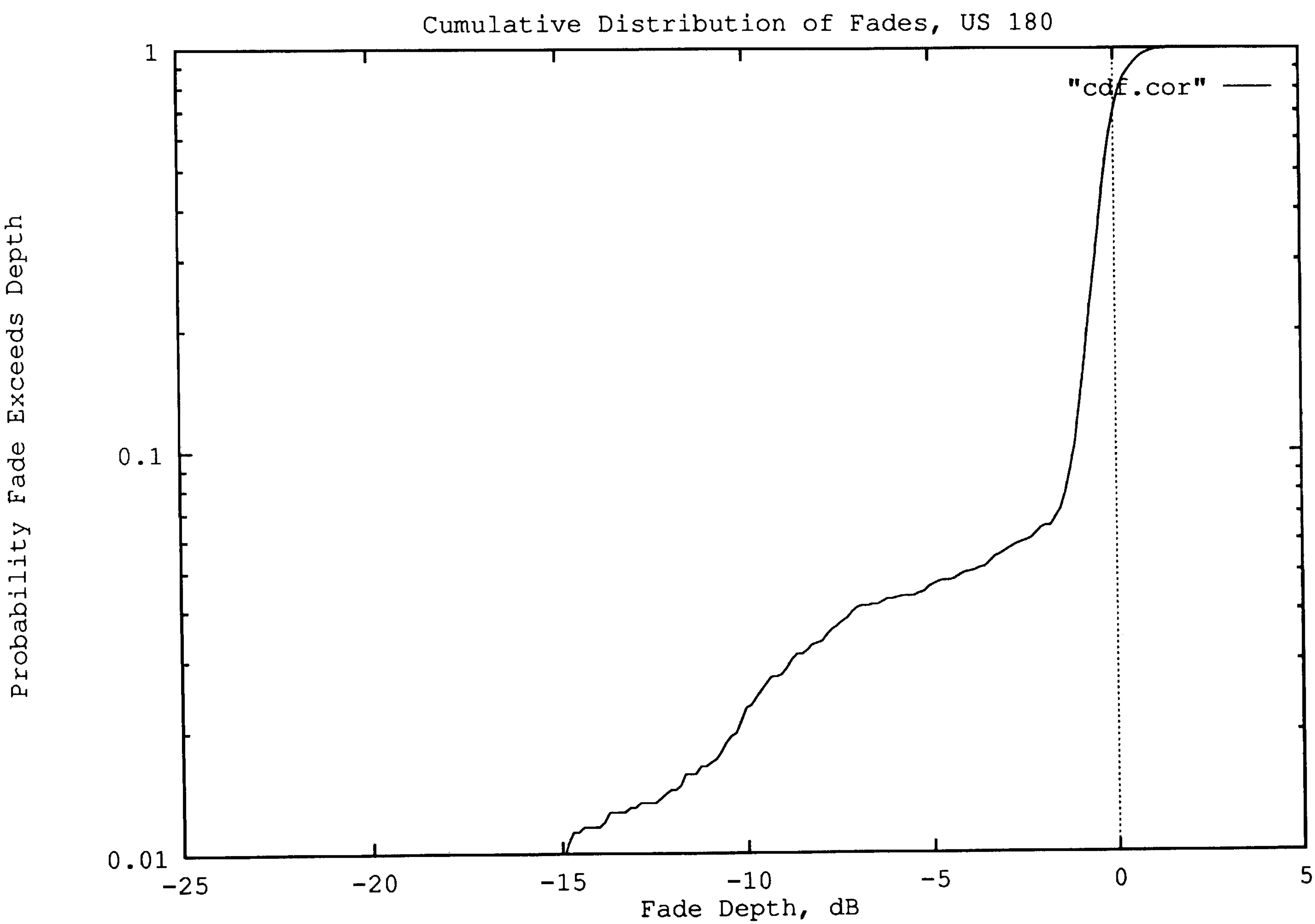
Cumulative Distribution of Fades, US 180
Probability Fade Exceeds Depth
Fade Depth, dB
"cdf.cor"
1
0.1
0.01
-25
-20
-15
-10
-5
0
5

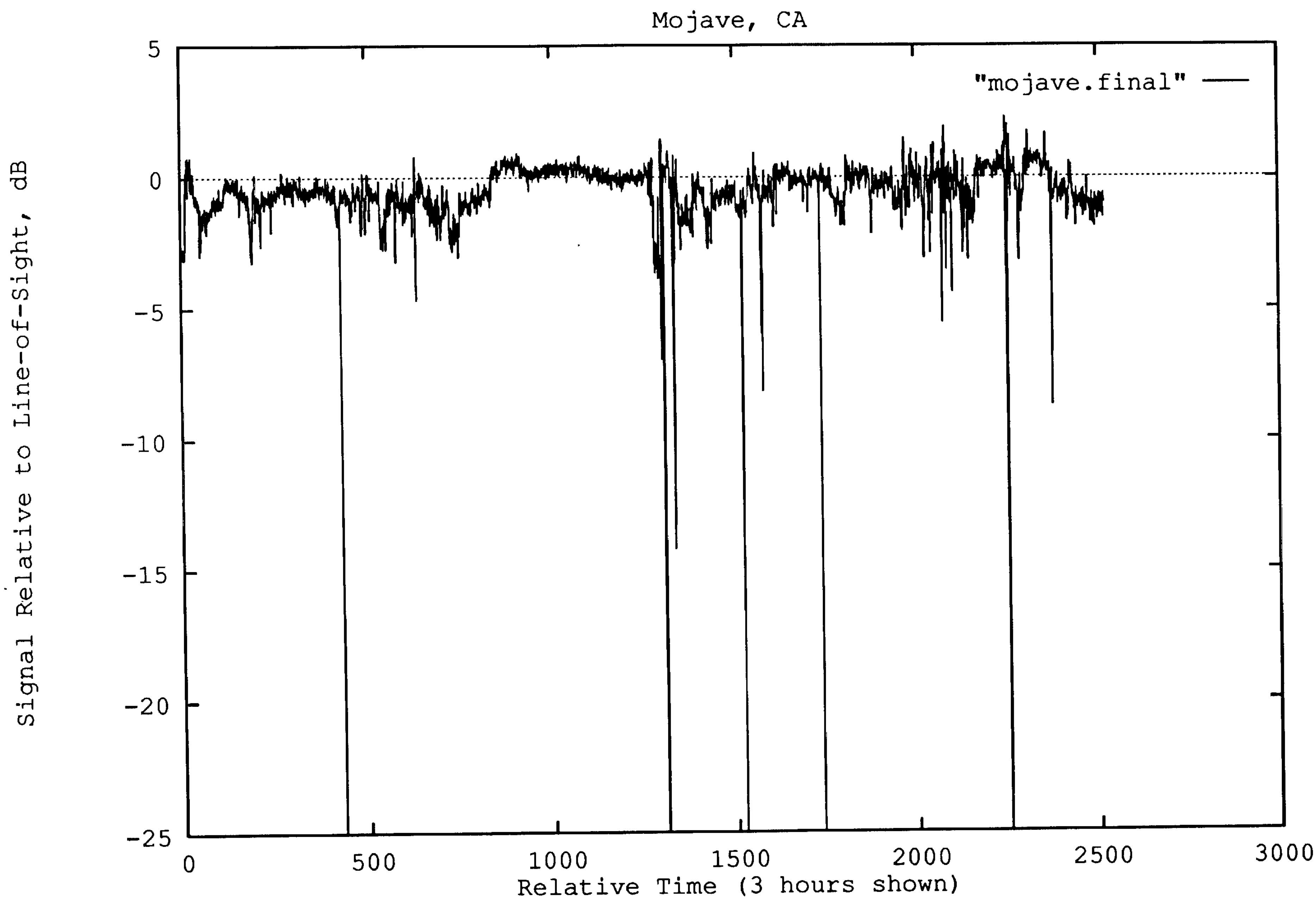

Mojave, CA
"mojave.final"
Signal Relative to Line-of-Sight, dB
5
0
-5
-10
-15
-20
-25
0
500
1000
1500
2000
2500
3000
Relative Time (3 hours shown)

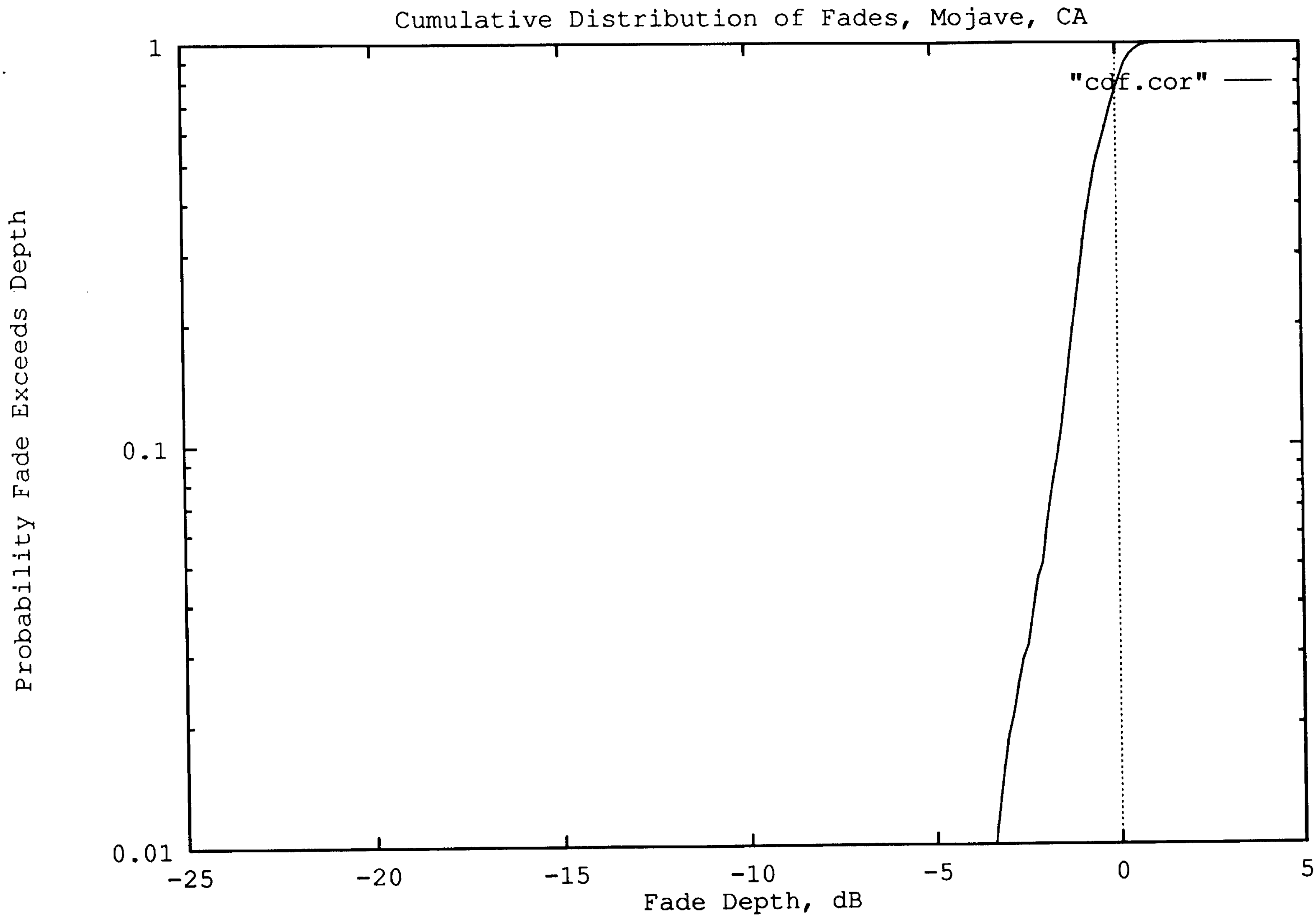

Cumulative Distribution of Fades, Mojave, CA
"cdf.cor"
Probability Fade Exceeds Depth
1
0.1
0.01
-25
-20
-15
-10
-5
0
5
Fade Depth, dB

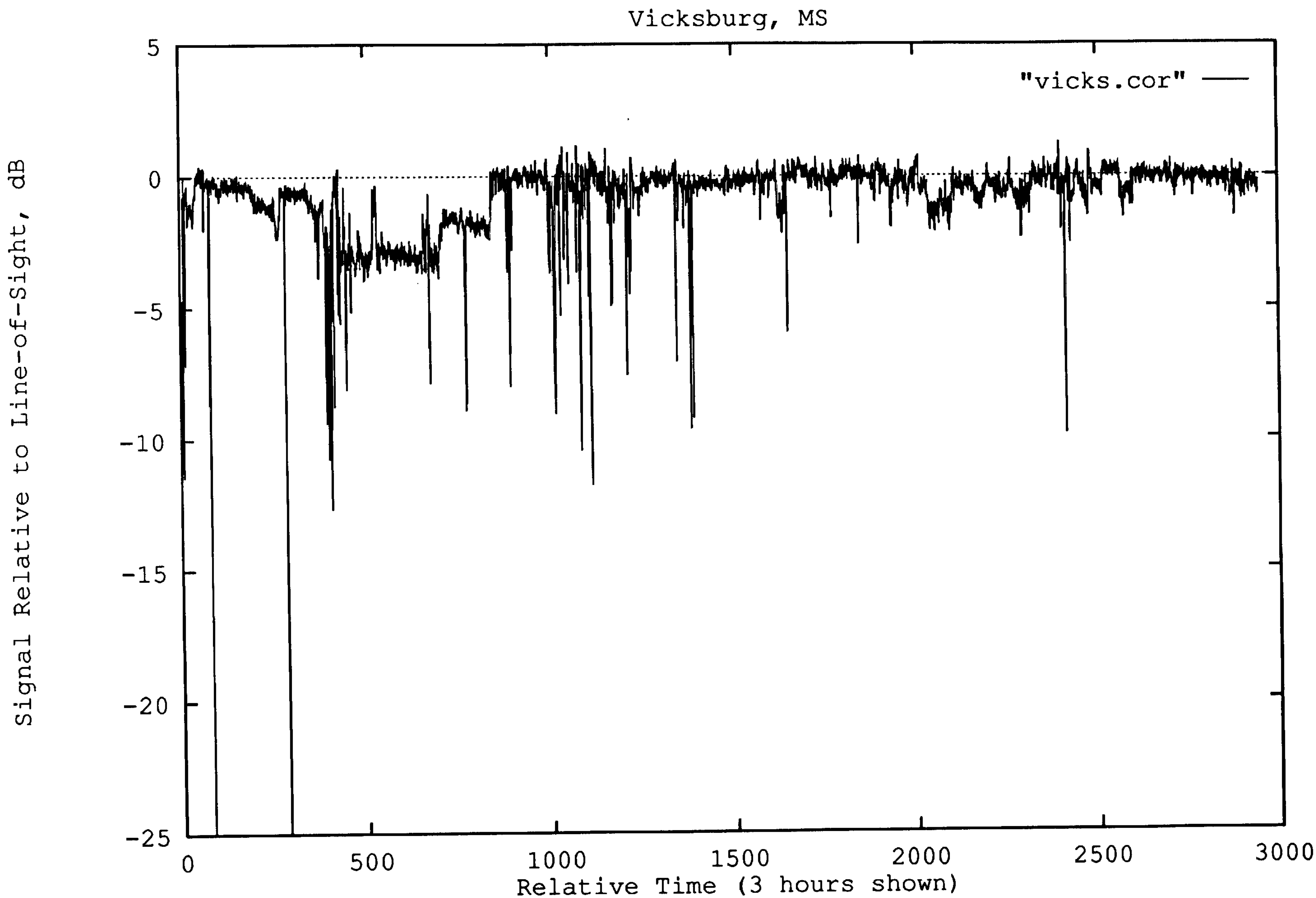

Vicksburg, MS
"vicks.cor"
Signal Relative to Line-of-Sight, dB
5
0
-5
-10
-15
-20
-25
0
500
1000
1500
2000
2500
3000
Relative Time (3 hours shown)

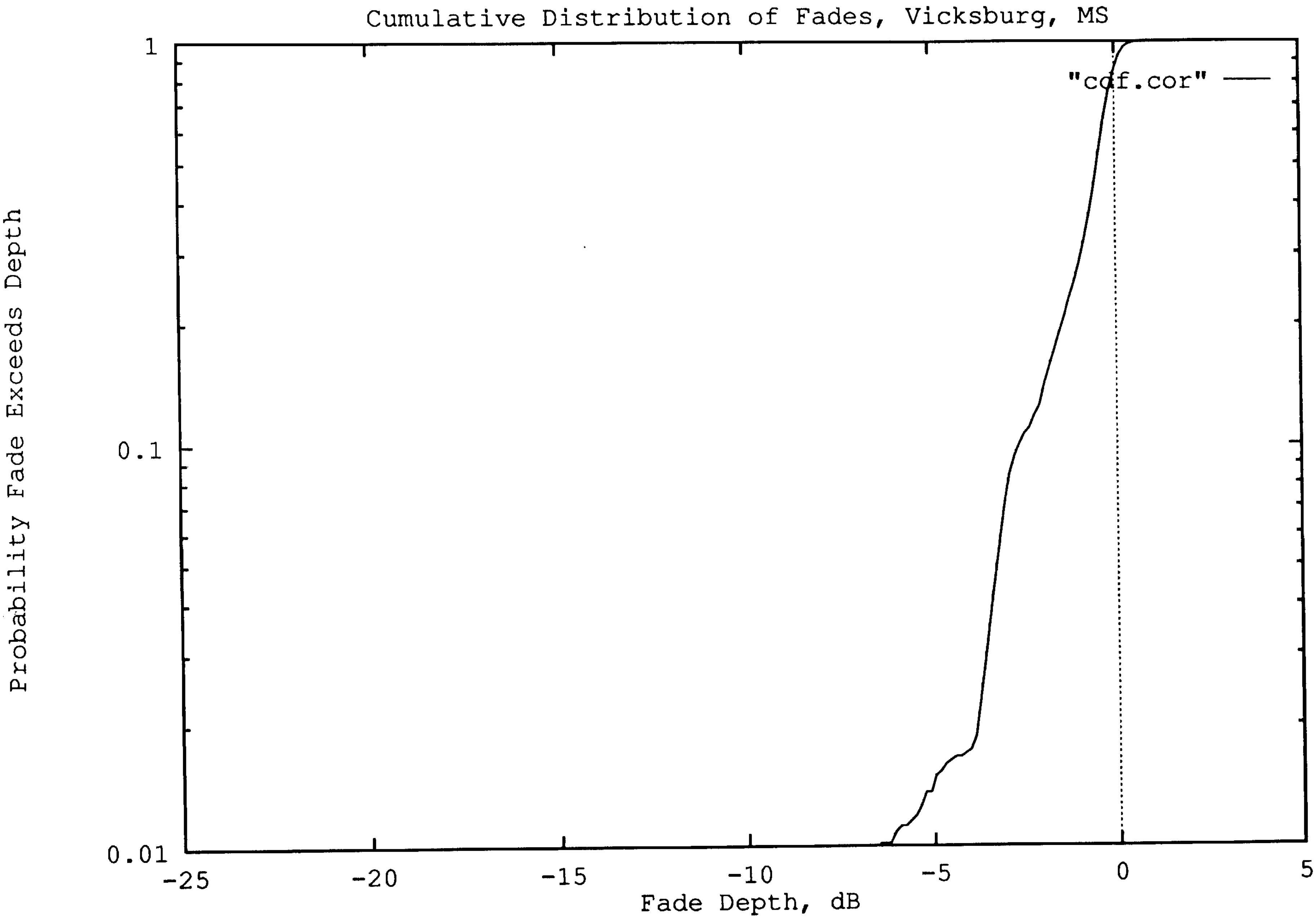

Cumulative Distribution of Fades, Vicksburg, MS
"cdf.cor"
Probability Fade Exceeds Depth
1
0.1
0.01
-25
-20
-15
-10
-5
0
5
Fade Depth, dB

Type II Shadowing

Pikes Peak, CO

Port Bolivar, TX to Port Arthur, LA

Katy, TX to Galveston, TX

Marshall, AR to Springdale, AR

Albuquerque, NM

Slidell, LA to Bolton, MS

Yellowstone N.P.

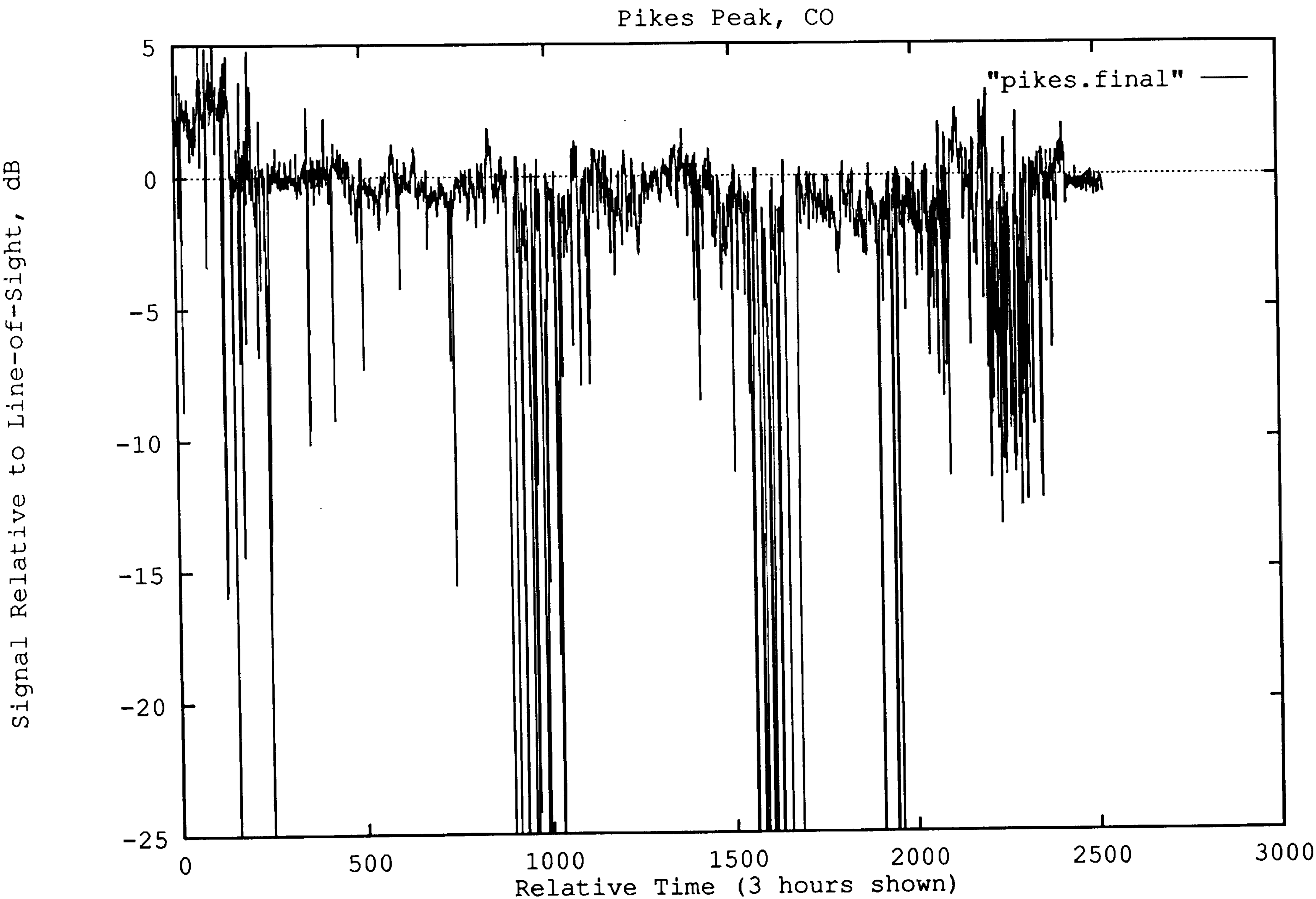

Pikes Peak, CO
"pikes.final"
Signal Relative to Line-of-Sight, dB
5
0
-5
-10
-15
-20
-25
0
500
1000
1500
2000
2500
3000
Relative Time (3 hours shown)

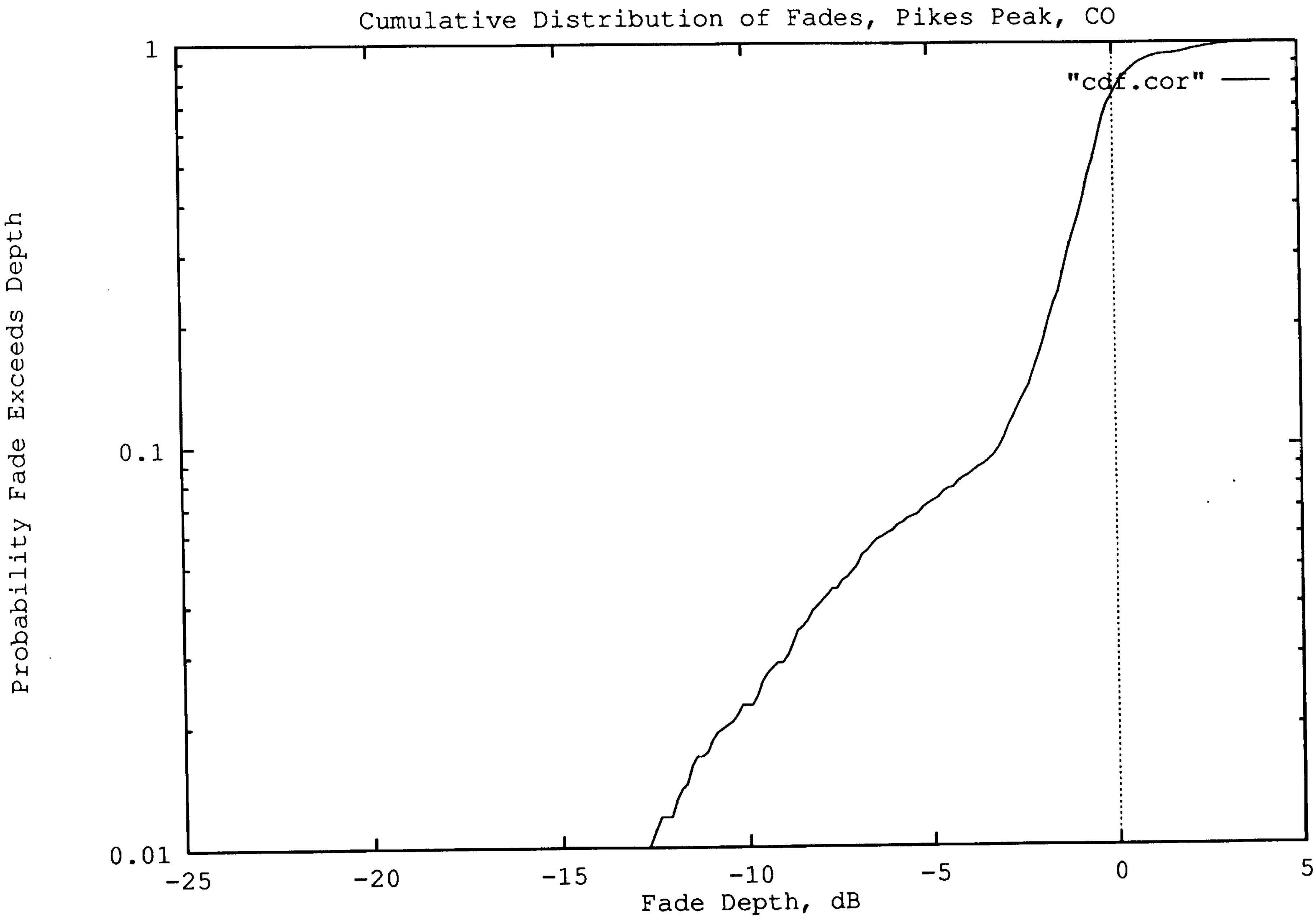

Cumulative Distribution of Fades, Pikes Peak, CO
"cdf.cor"
1
0.1
0.01
Probability Fade Exceeds Depth
-25
-20
-15
-10
-5
0
5
Fade Depth, dB

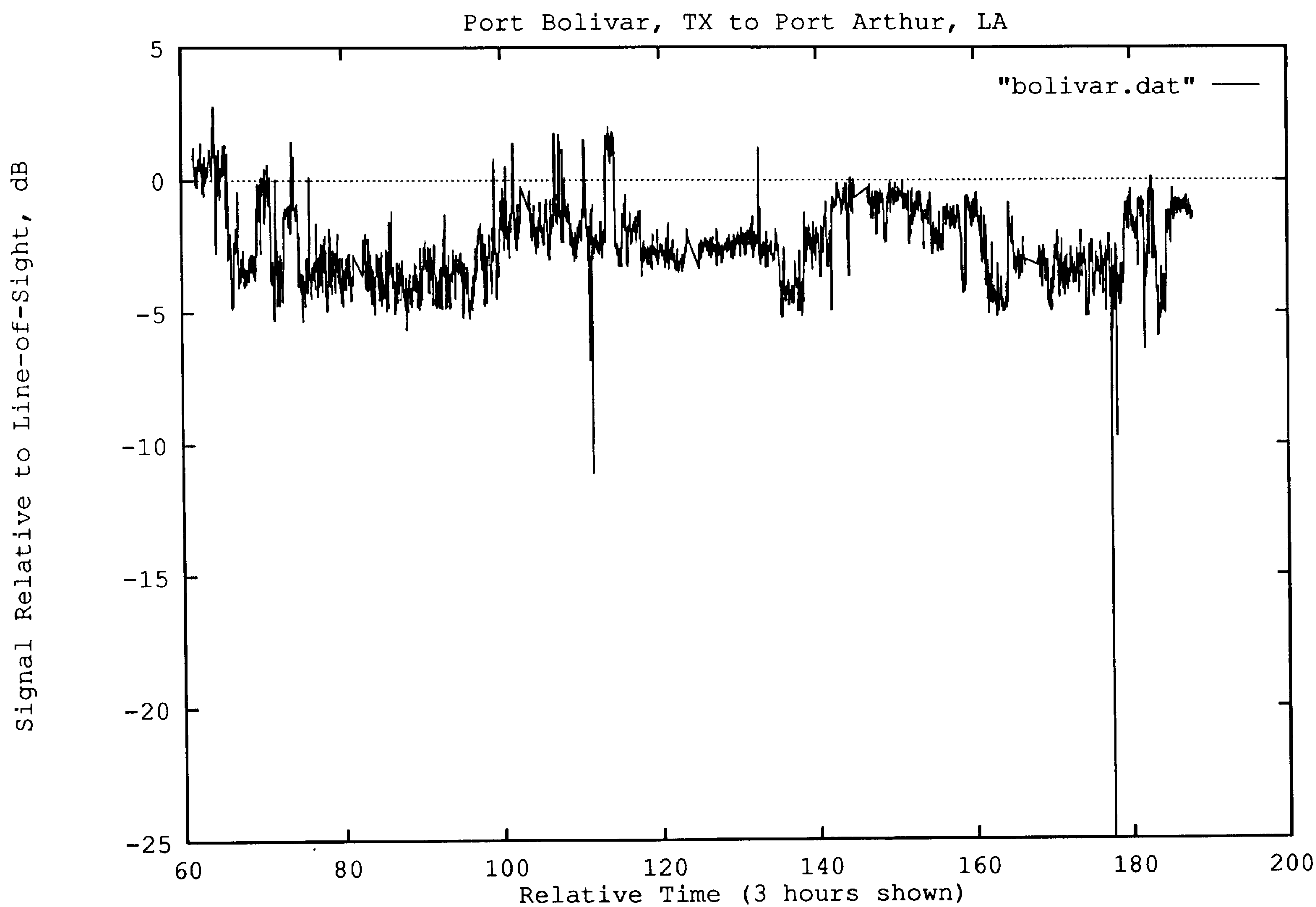
Port Bolivar, TX to Port Arthur, LA
"bolivar.dat"
Signal Relative to Line-of-Sight, dB
5
0
-5
-10
-15
-20
-25
60
80
100
120
140
160
180
200
Relative Time (3 hours shown)

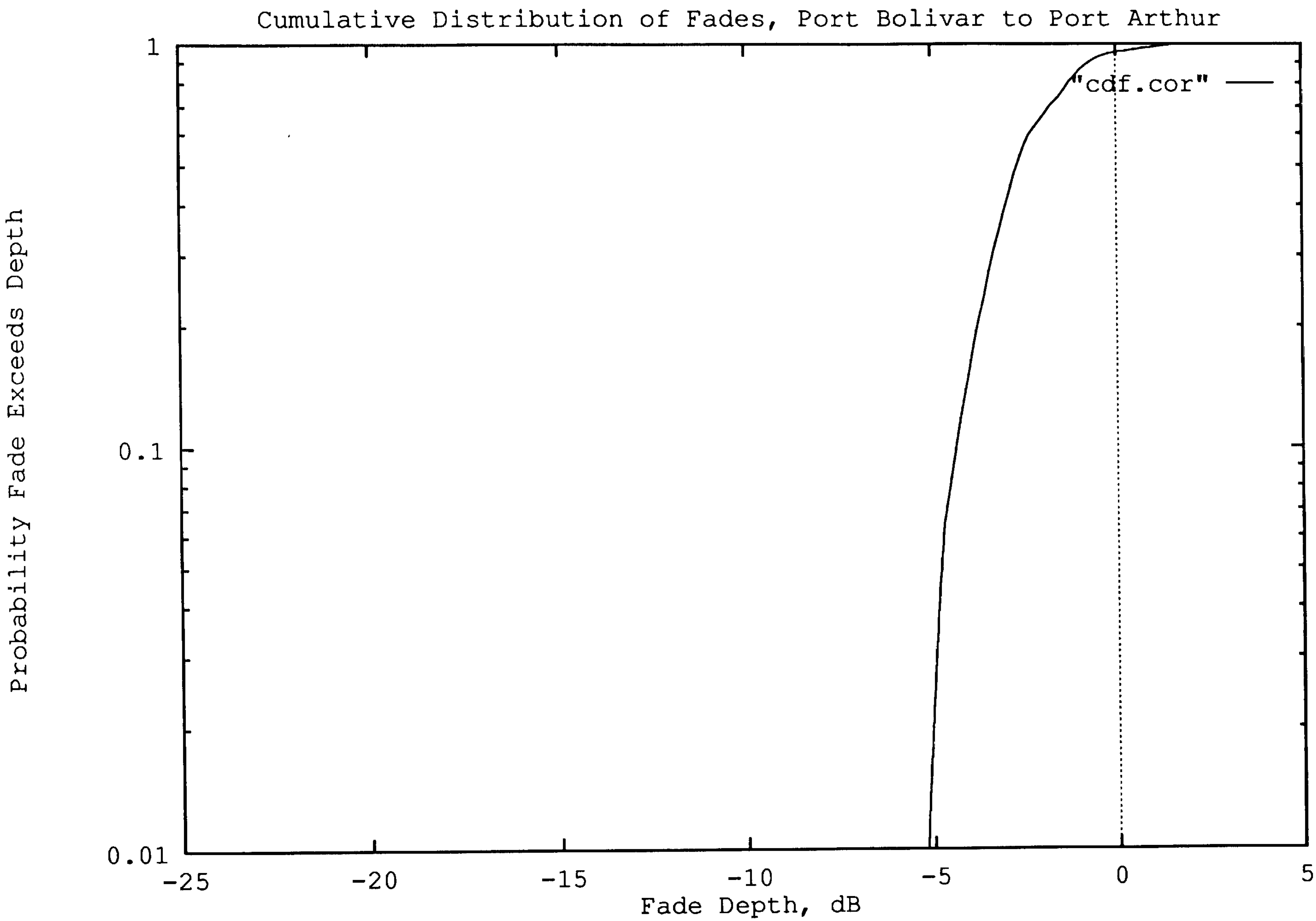
Cumulative Distribution of Fades, Port Bolivar to Port Arthur
"cdf.cor"
Probability Fade Exceeds Depth
1
0.1
0.01
-25
-20
-15
-10
-5
0
5
Fade Depth, dB

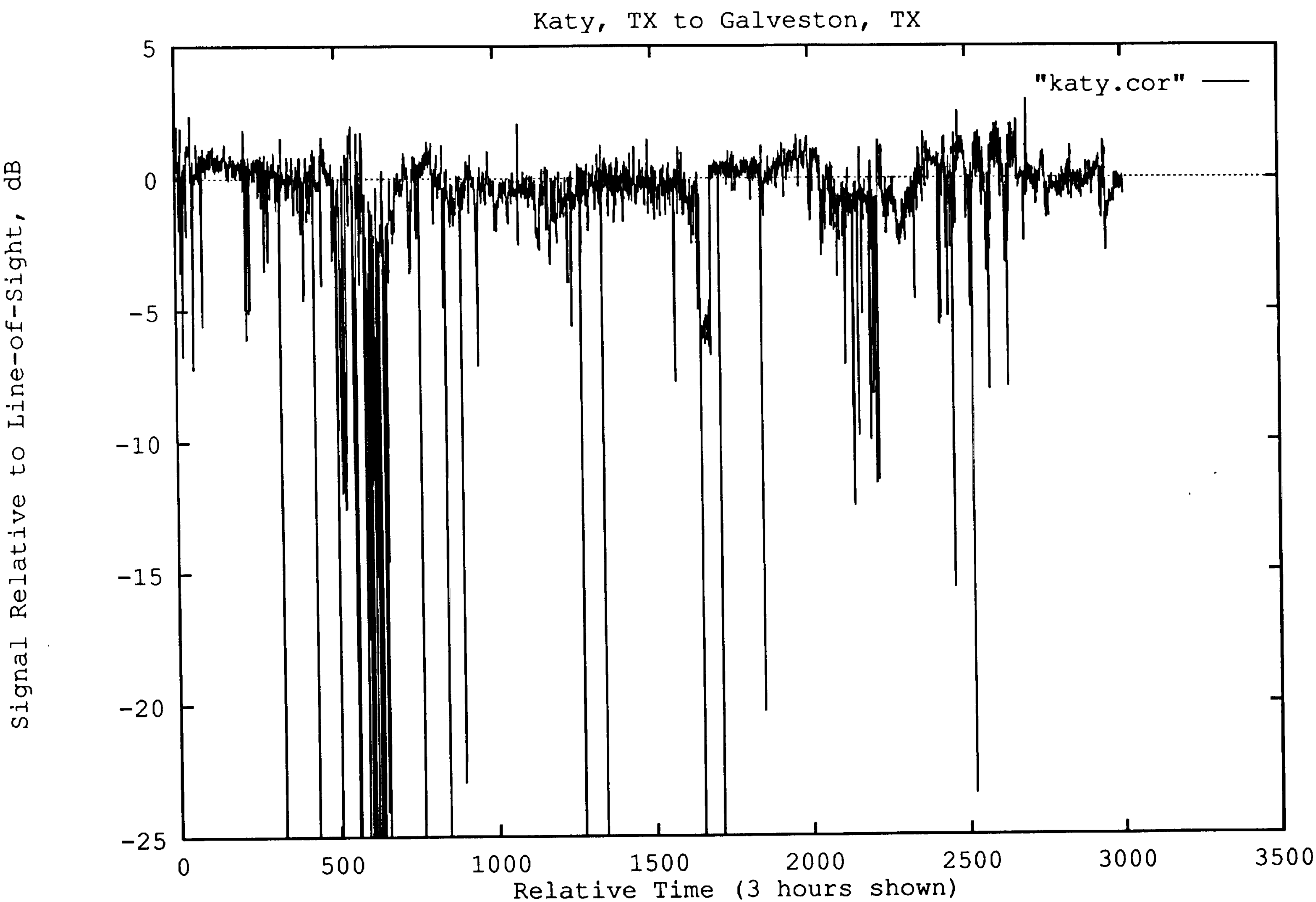
Katy, TX to Galveston, TX
"katy.cor"
Signal Relative to Line-of-Sight, dB
5
0
-5
-10
-15
-20
-25
0
500
1000
1500
2000
2500
3000
3500
Relative Time (3 hours shown)

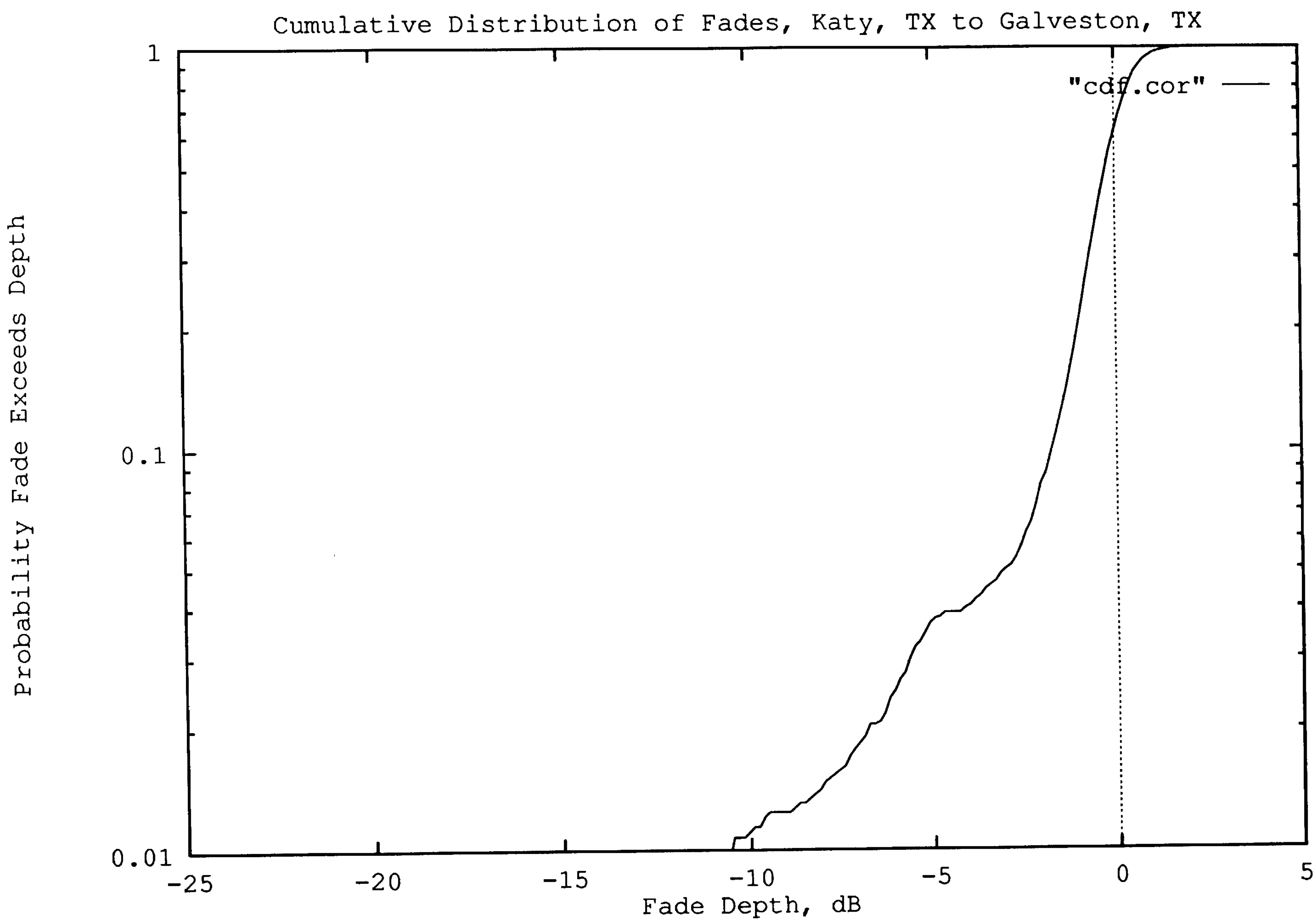

Cumulative Distribution of Fades, Katy, TX to Galveston, TX
"cdf.cor"
Probability Fade Exceeds Depth
1
0.1
0.01
-25
-20
-15
-10
-5
0
5
Fade Depth, dB

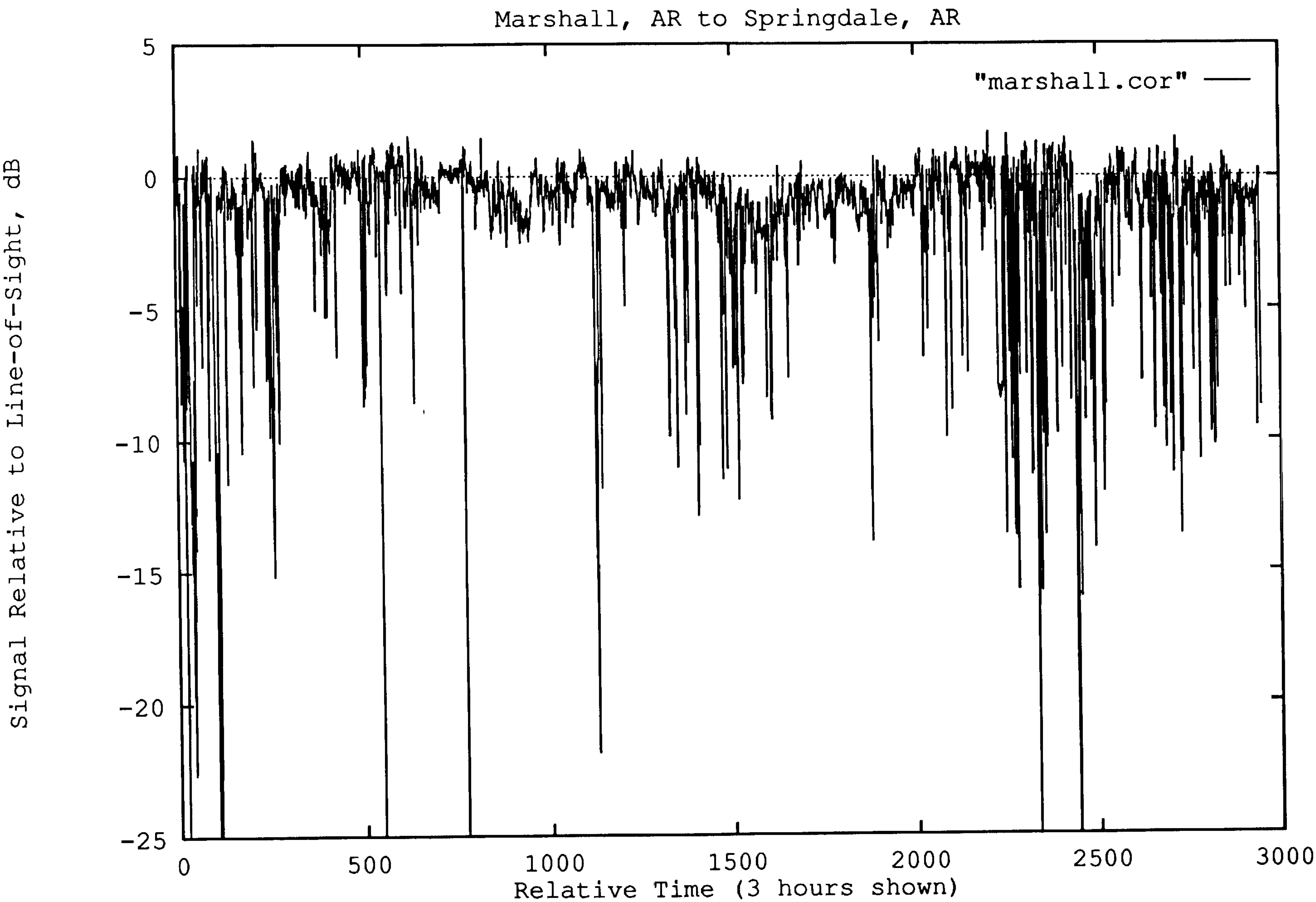

Marshall, AR to Springdale, AR
"marshall.cor"
Signal Relative to Line-of-Sight, dB
5
0
-5
-10
-15
-20
-25
0
500
1000
1500
2000
2500
3000
Relative Time (3 hours shown)

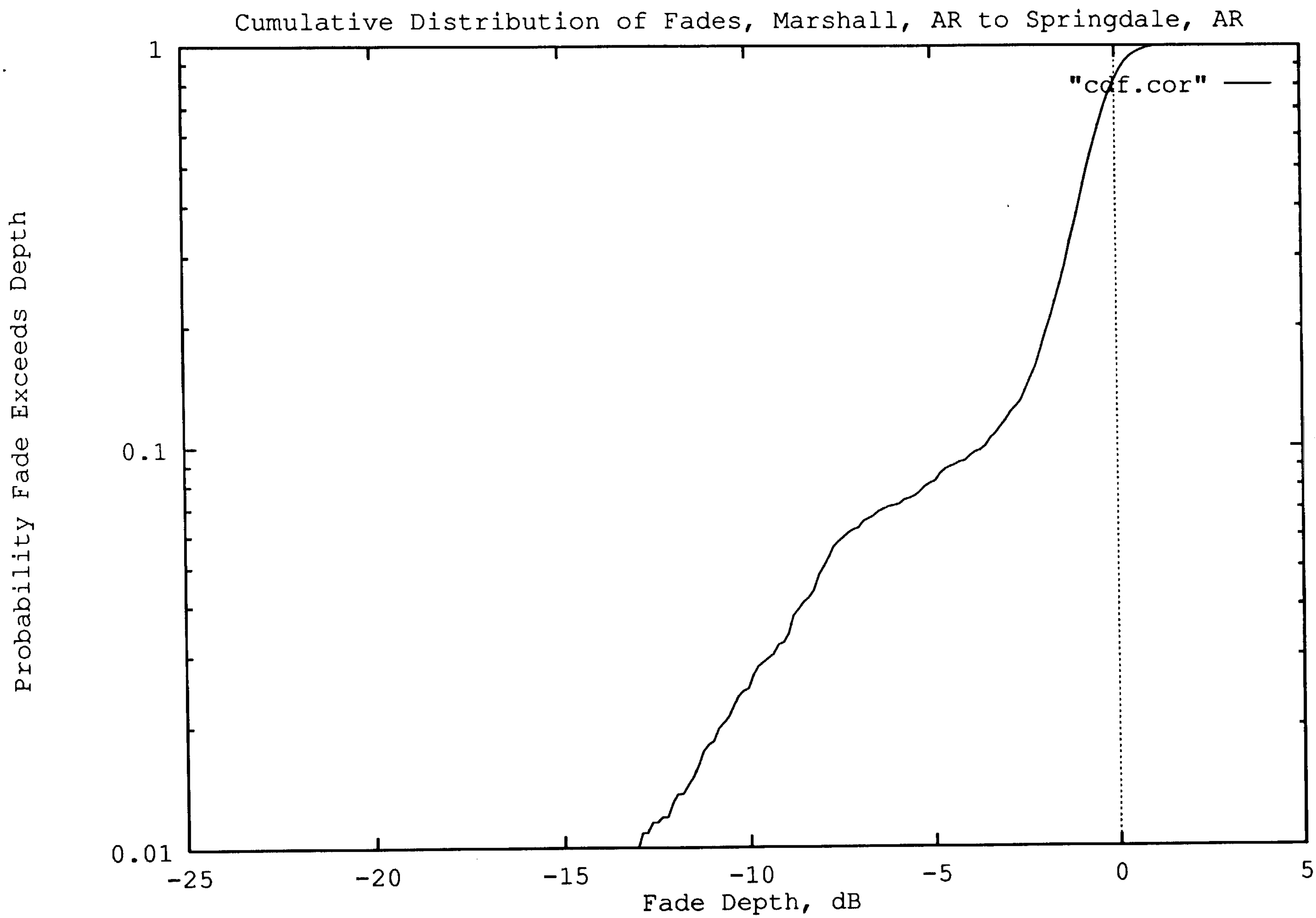

Cumulative Distribution of Fades, Marshall, AR to Springdale, AR
Probability Fade Exceeds Depth
Fade Depth, dB
"cdf.cor"
1
0.1
0.01
-25
-20
-15
-10
-5
0
5

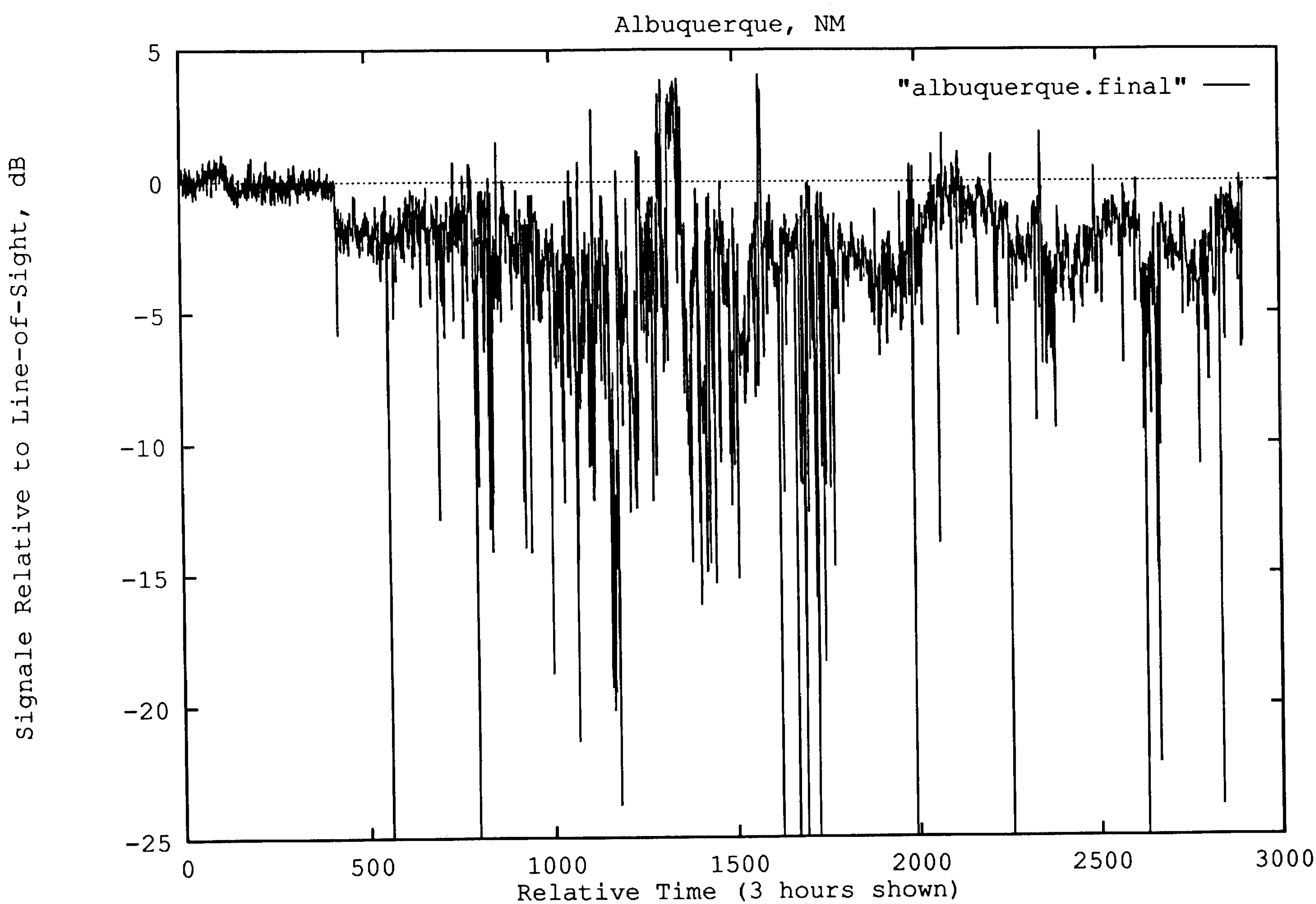

Albuquerque, NM
"albuquerque.final"
Signale Relative to Line-of-Sight, dB
5
0
-5
-10
-15
-20
-25
0
500
1000
1500
2000
2500
3000
Relative Time (3 hours shown)

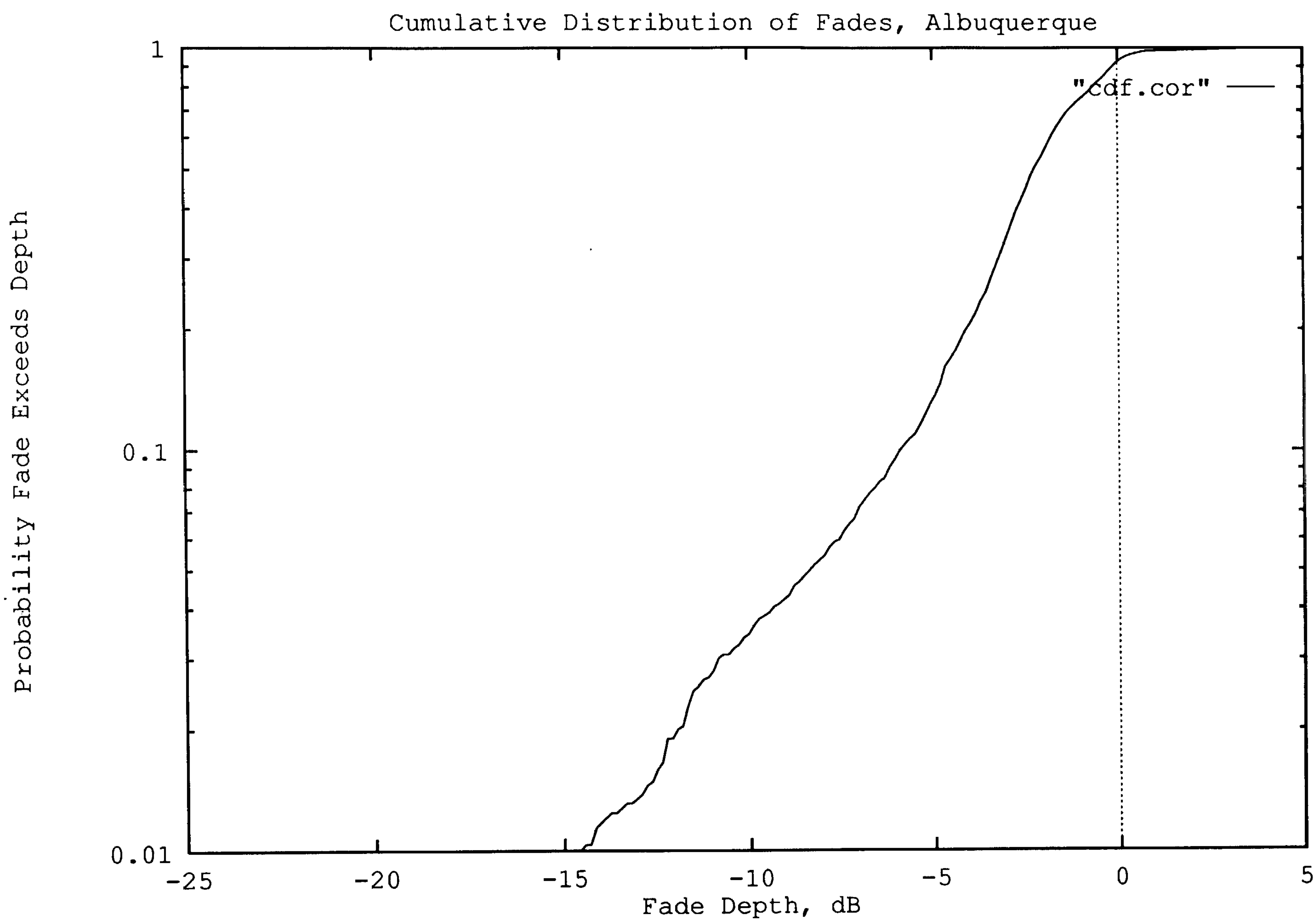

Cumulative Distribution of Fades, Albuquerque
"cdf.cor"
Probability Fade Exceeds Depth
1
0.1
0.01
-25
-20
-15
-10
-5
0
5
Fade Depth, dB

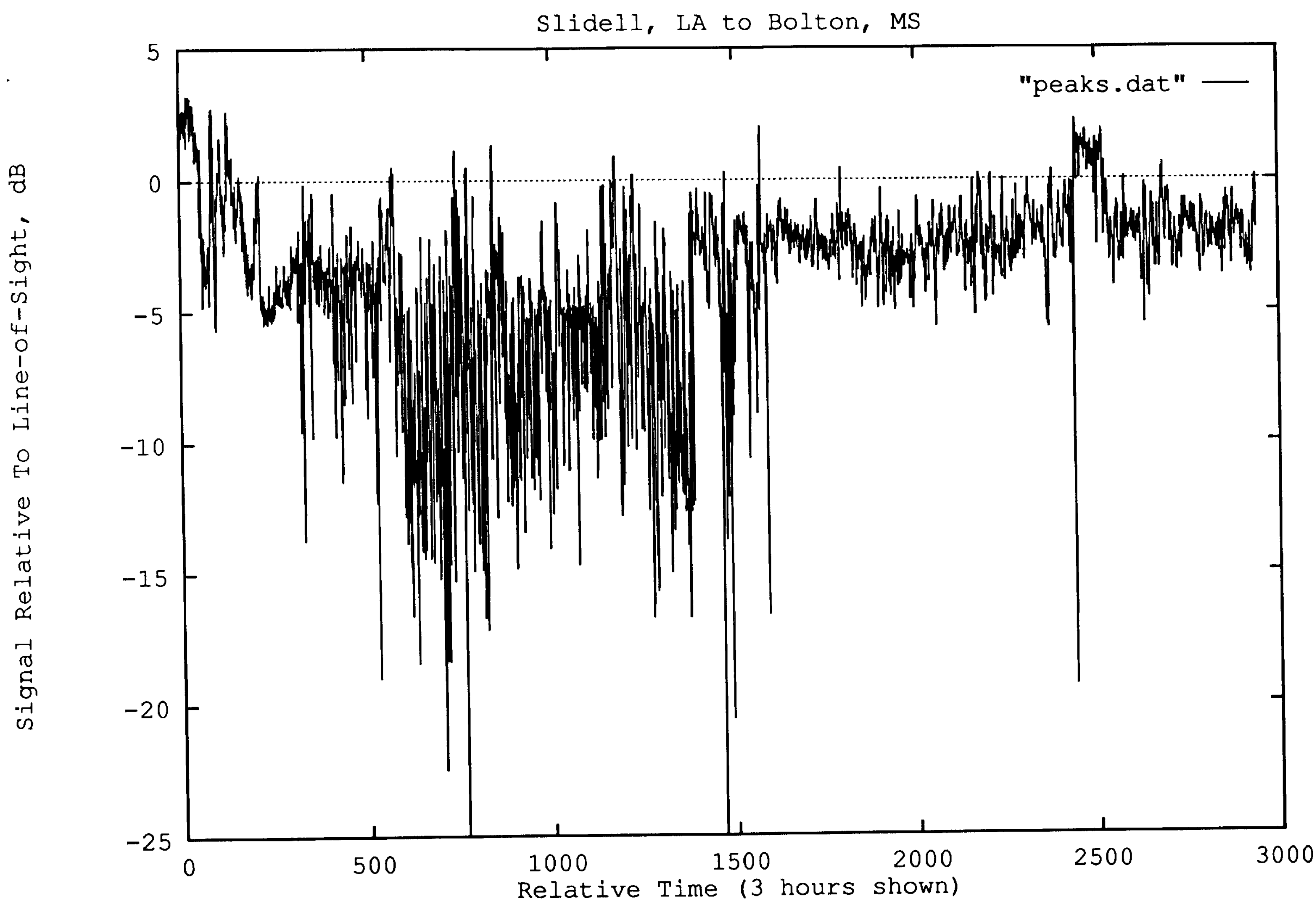
Slidell, LA to Bolton, MS
"peaks.dat"
Signal Relative To Line-of-Sight, dB
5
0
-5
-10
-15
-20
-25
0
500
1000
1500
2000
2500
3000
Relative Time (3 hours shown)

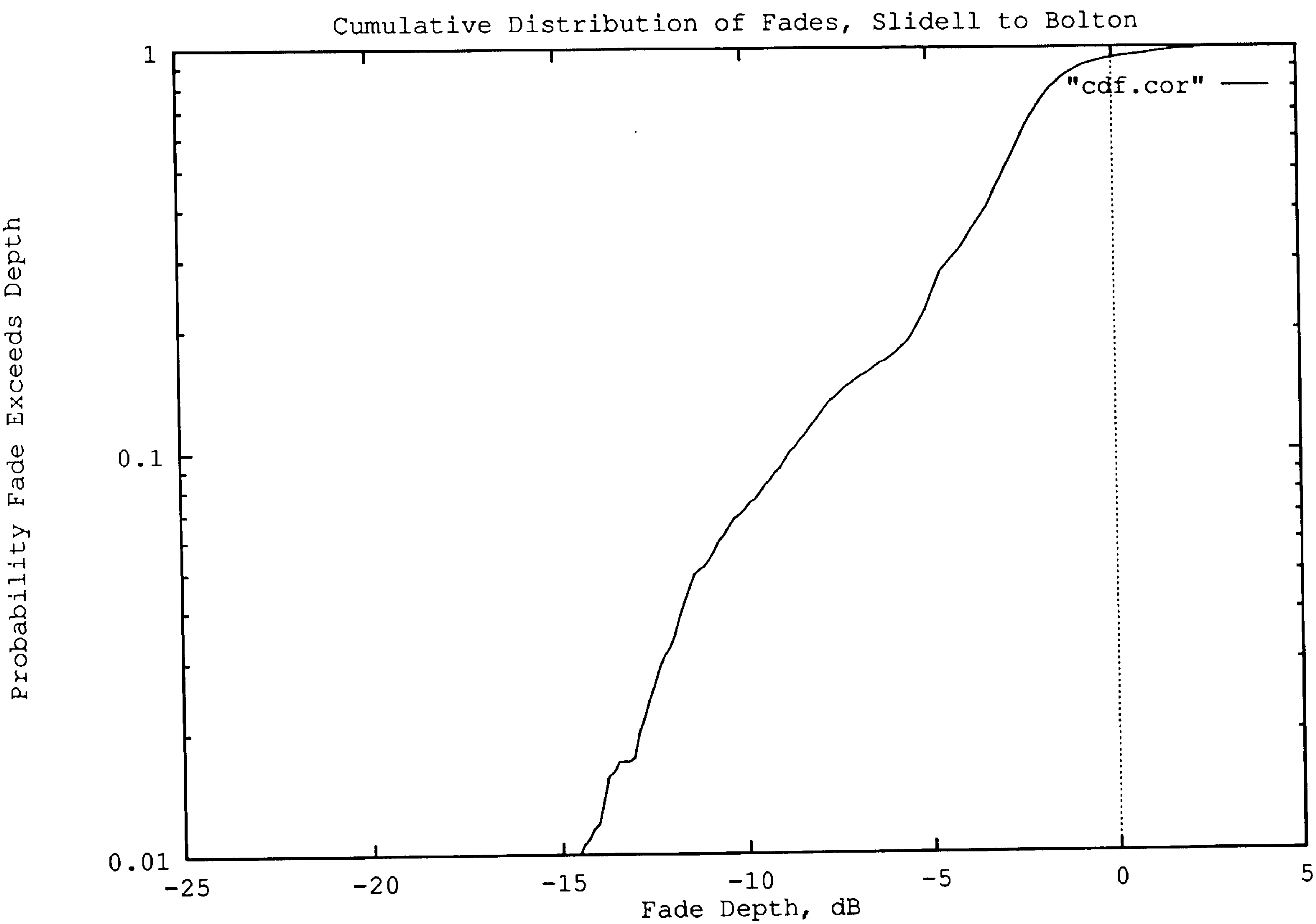
Cumulative Distribution of Fades, Slidell to Bolton
"cdf.cor"
Probability Fade Exceeds Depth
1
0.1
0.01
-25
-20
-15
-10
-5
0
5
Fade Depth, dB

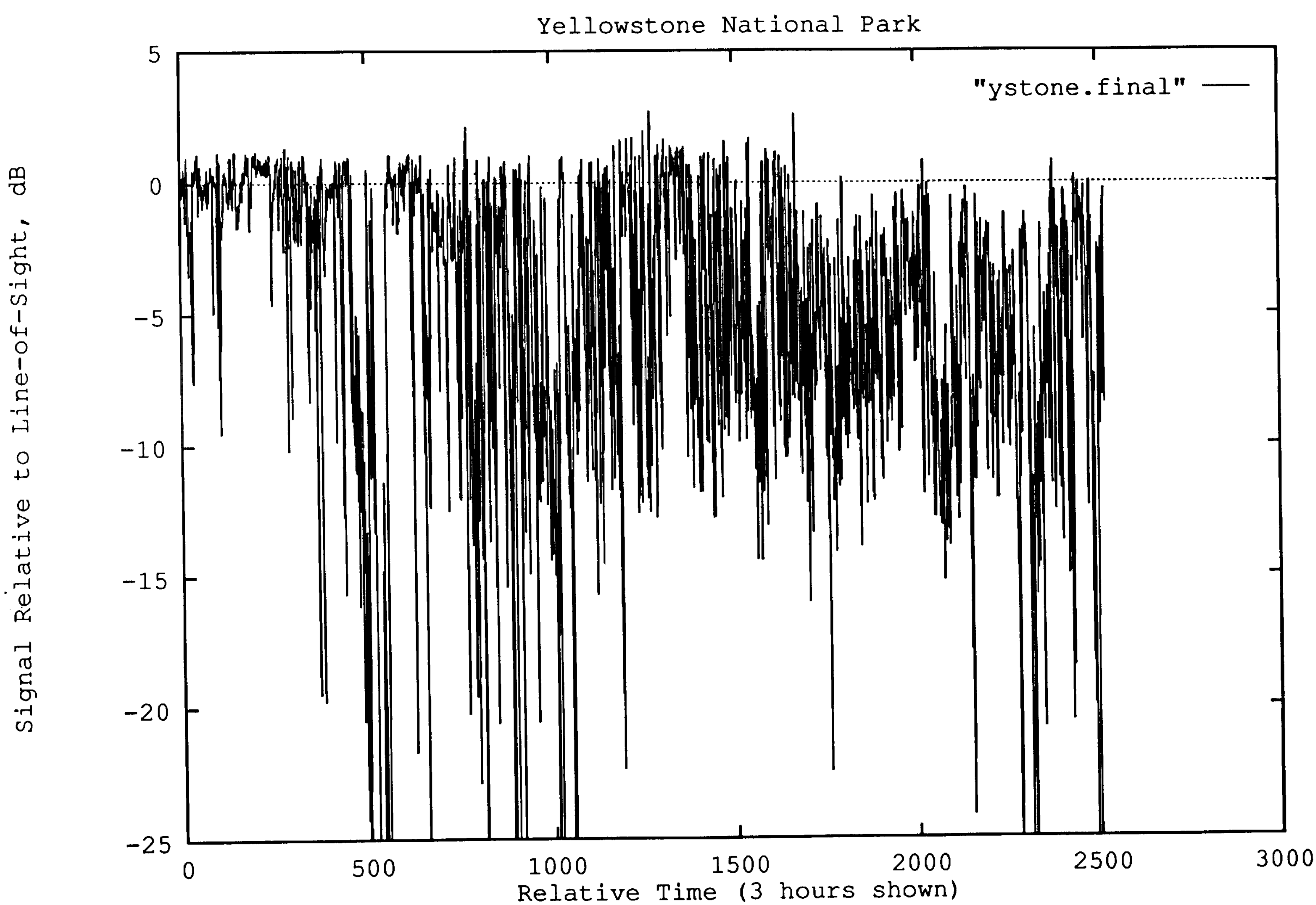

Yellowstone National Park
"ystone.final"
Signal Relative to Line-of-Sight, dB
5
0
-5
-10
-15
-20
-25
0
500
1000
1500
2000
2500
3000
Relative Time (3 hours shown)

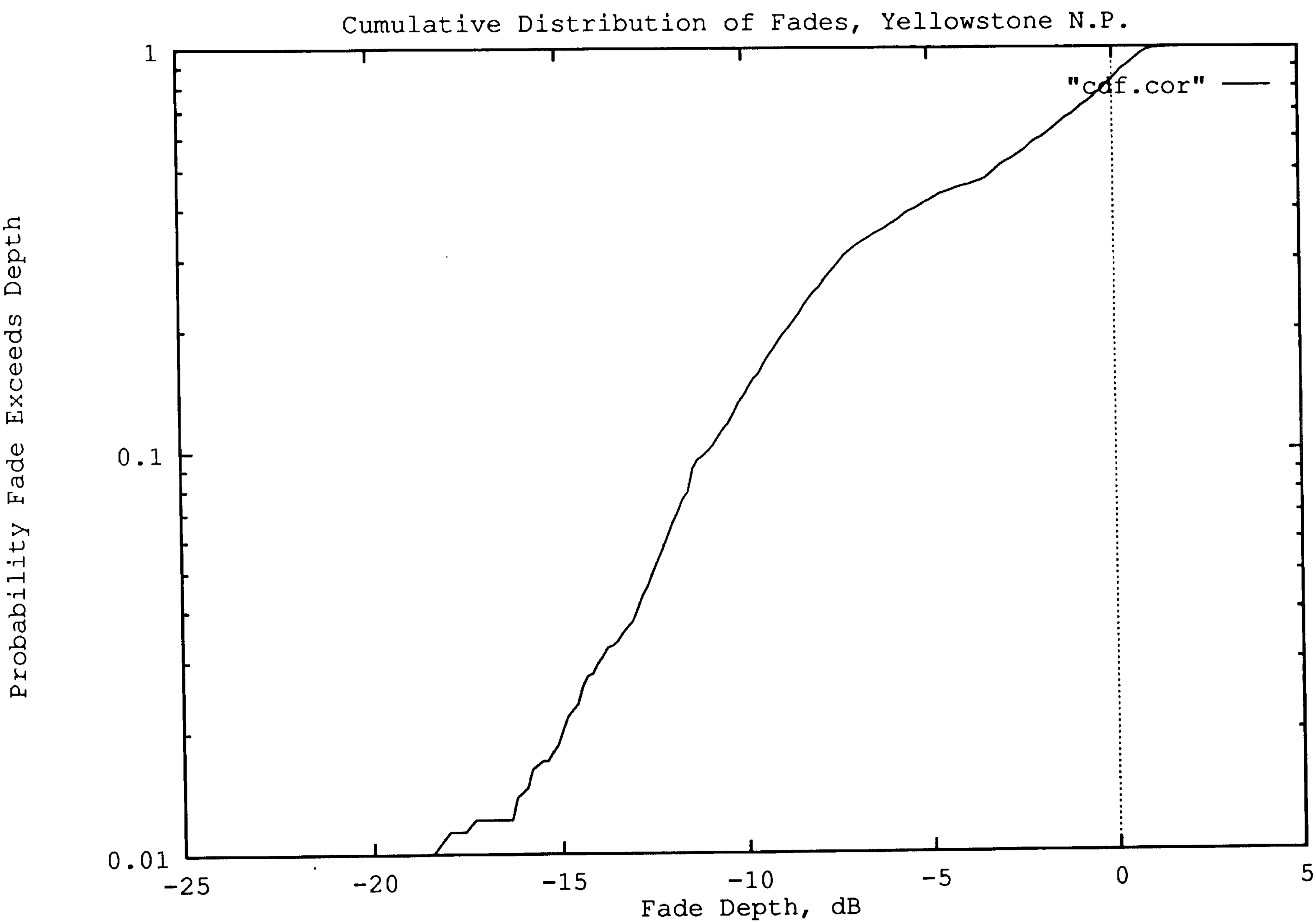
Cumulative Distribution of Fades, Yellowstone N.P.
"cdf.cor"
Probability Fade Exceeds Depth
1
0.1
0.01
-25
-20
-15
-10
-5
0
5
Fade Depth, dB

Type III Shadowing

Olympic National Park

Yosemite National Park

Sequoia National Park

Denver, CO

Portland, OR

San Francisco, CA

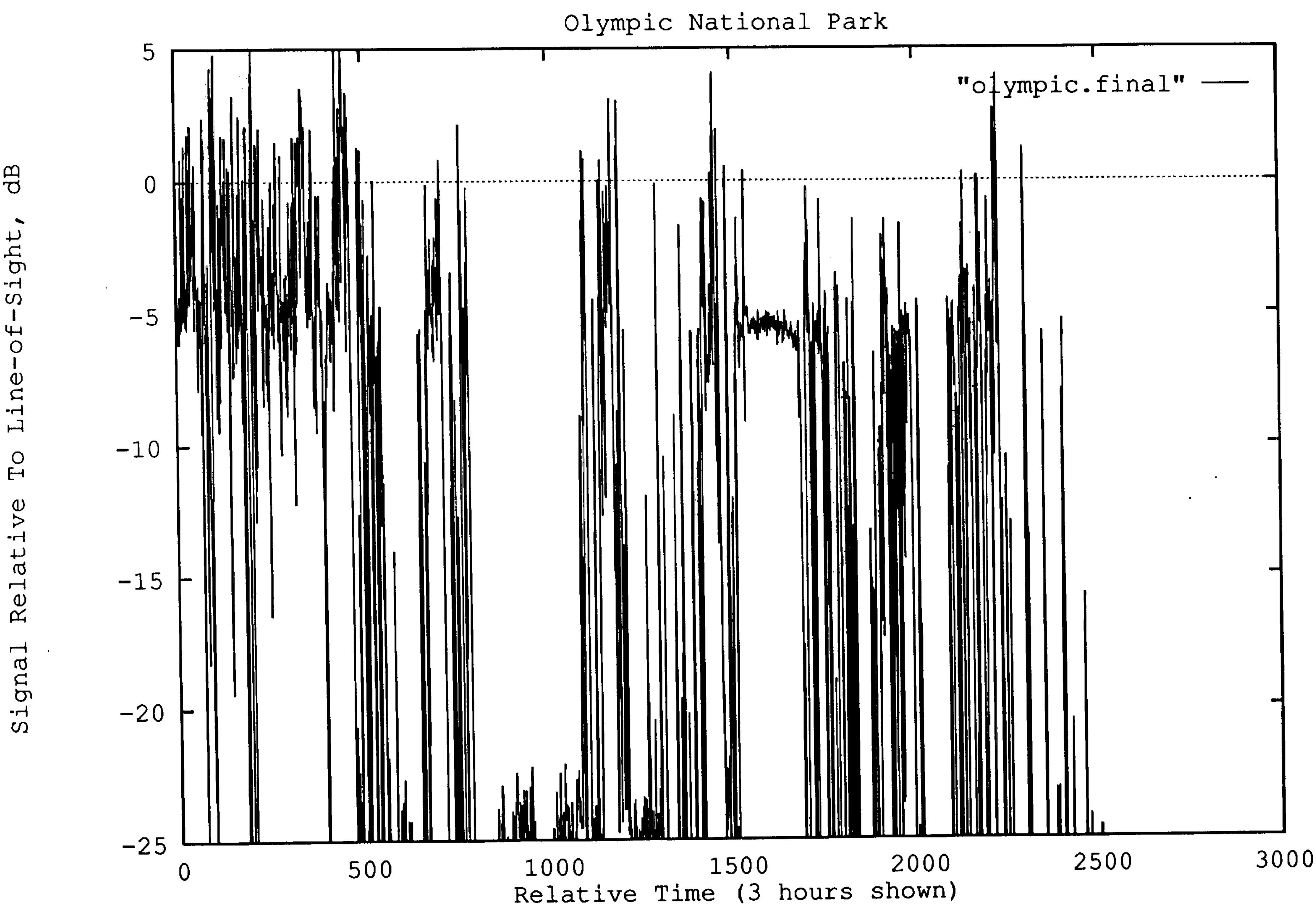

Olympic National Park
"olympic.final"
Signal Relative To Line-of-Sight, dB
5
0
-5
-10
-15
-20
-25
0
500
1000
1500
2000
2500
3000
Relative Time (3 hours shown)

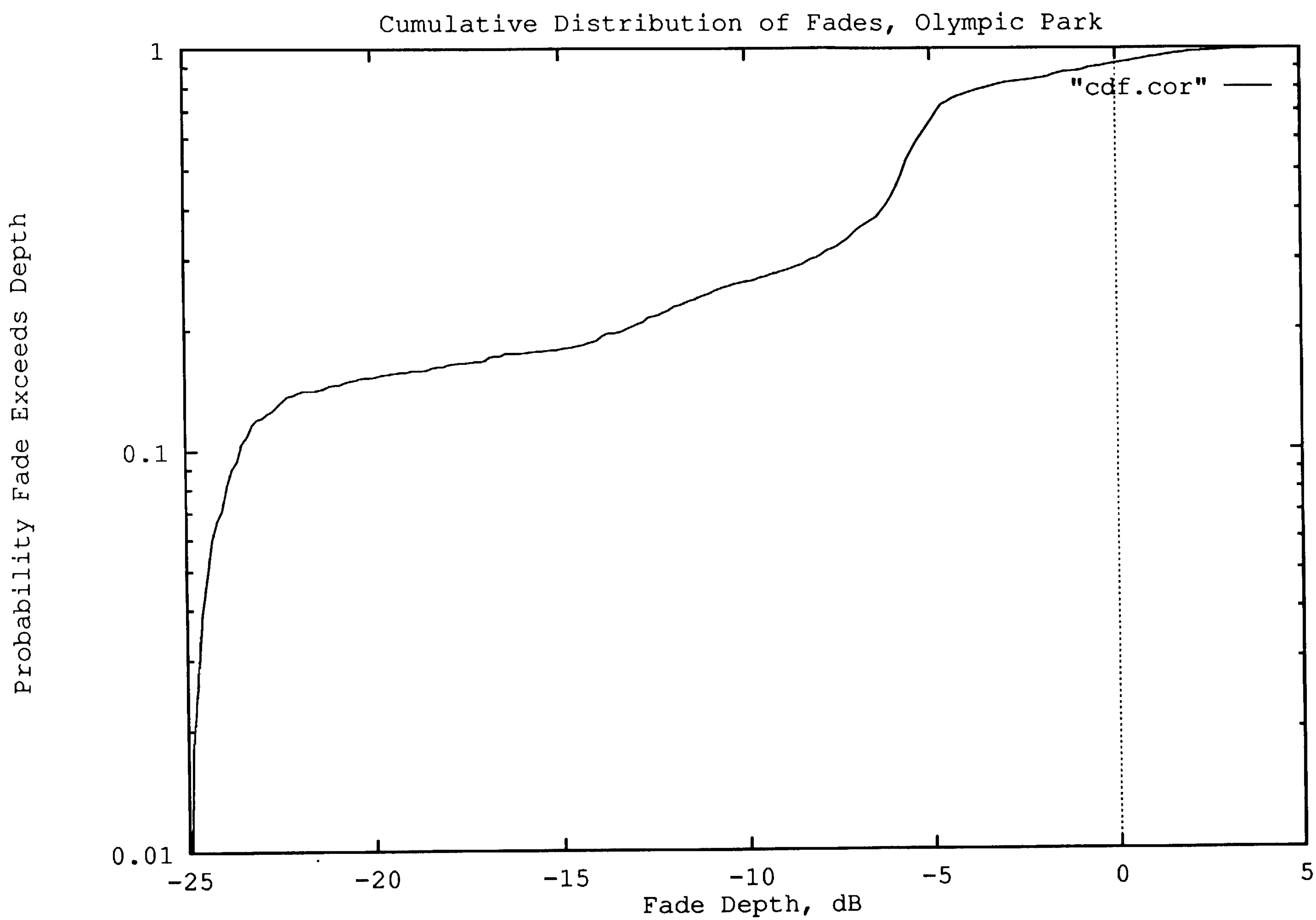

Cumulative Distribution of Fades, Olympic Park
"cdf.cor"
Probability Fade Exceeds Depth
1
0.1
0.01
-25
-20
-15
-10
-5
0
5
Fade Depth, dB

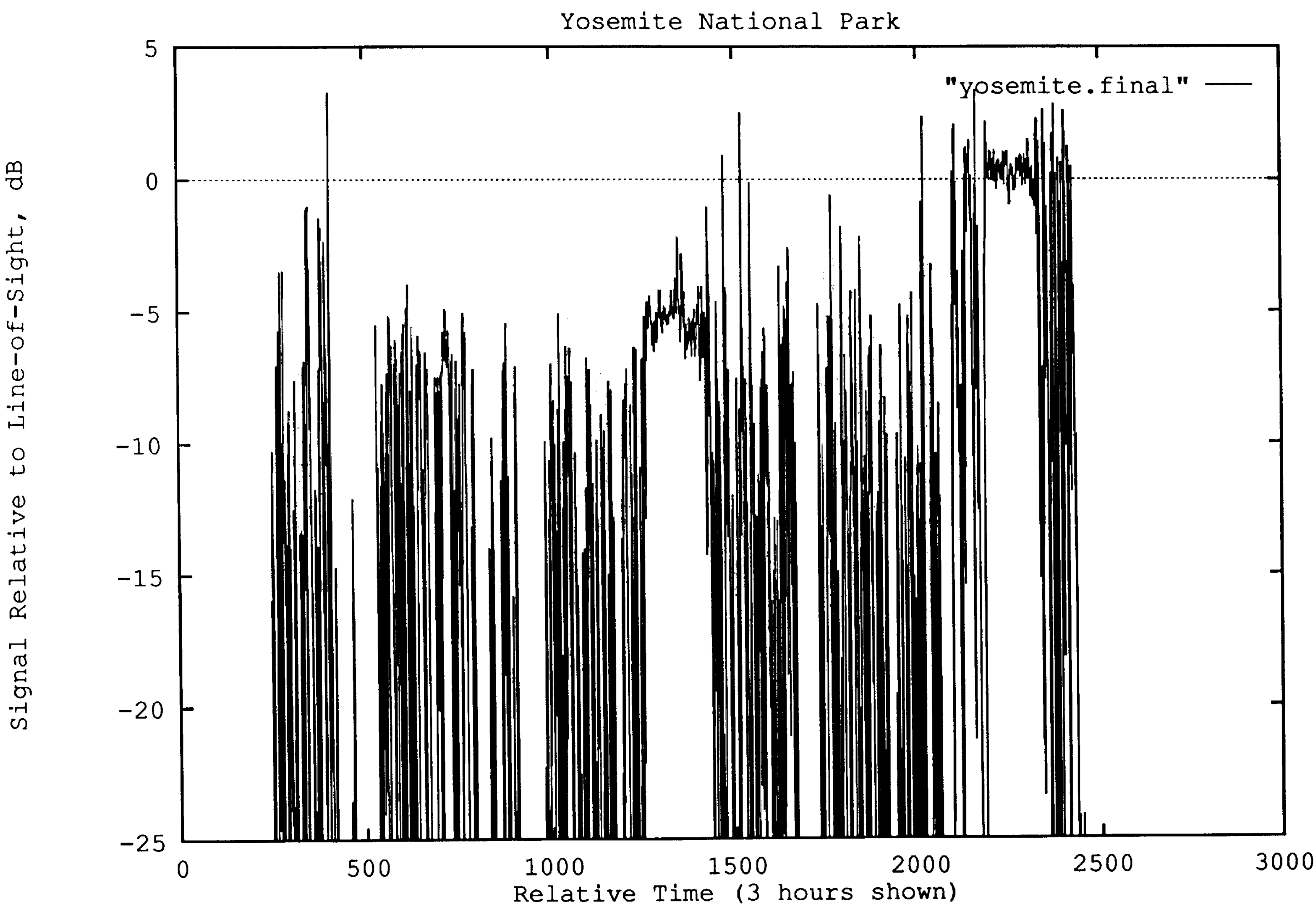
Yosemite National Park
"yosemite.final"
Signal Relative to Line-of-Sight, dB
5
0
-5
-10
-15
-20
-25
0
500
1000
1500
2000
2500
3000
Relative Time (3 hours shown)

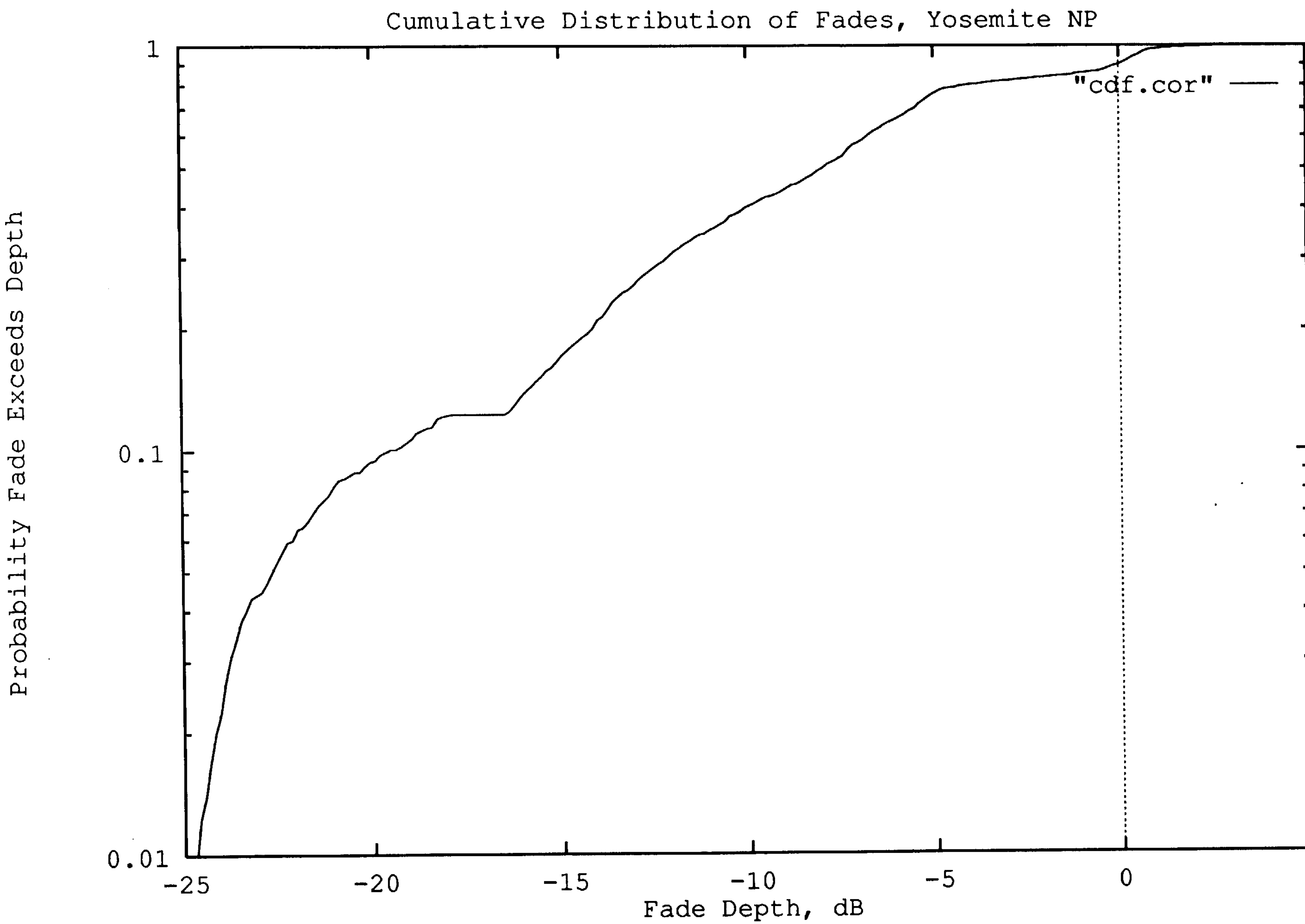

Cumulative Distribution of Fades, Yosemite NP
"cdf.cor"
Probability Fade Exceeds Depth
1
0.1
0.01
-25
-20
-15
-10
-5
0
5
Fade Depth, dB

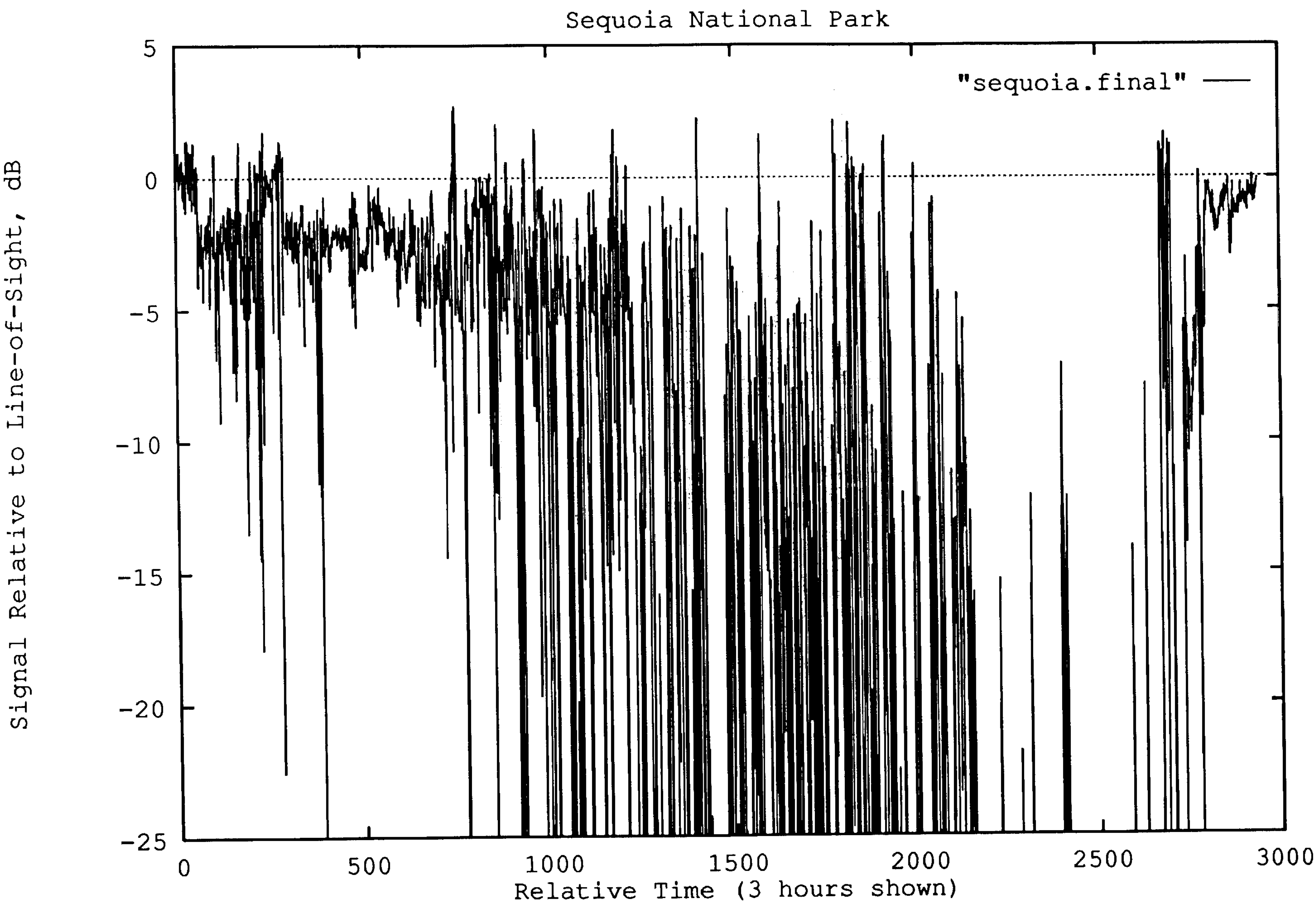

Sequoia National Park
"sequoia.final"
Signal Relative to Line-of-Sight, dB
5
0
-5
-10
-15
-20
-25
0
500
1000
1500
2000
2500
3000
Relative Time (3 hours shown)

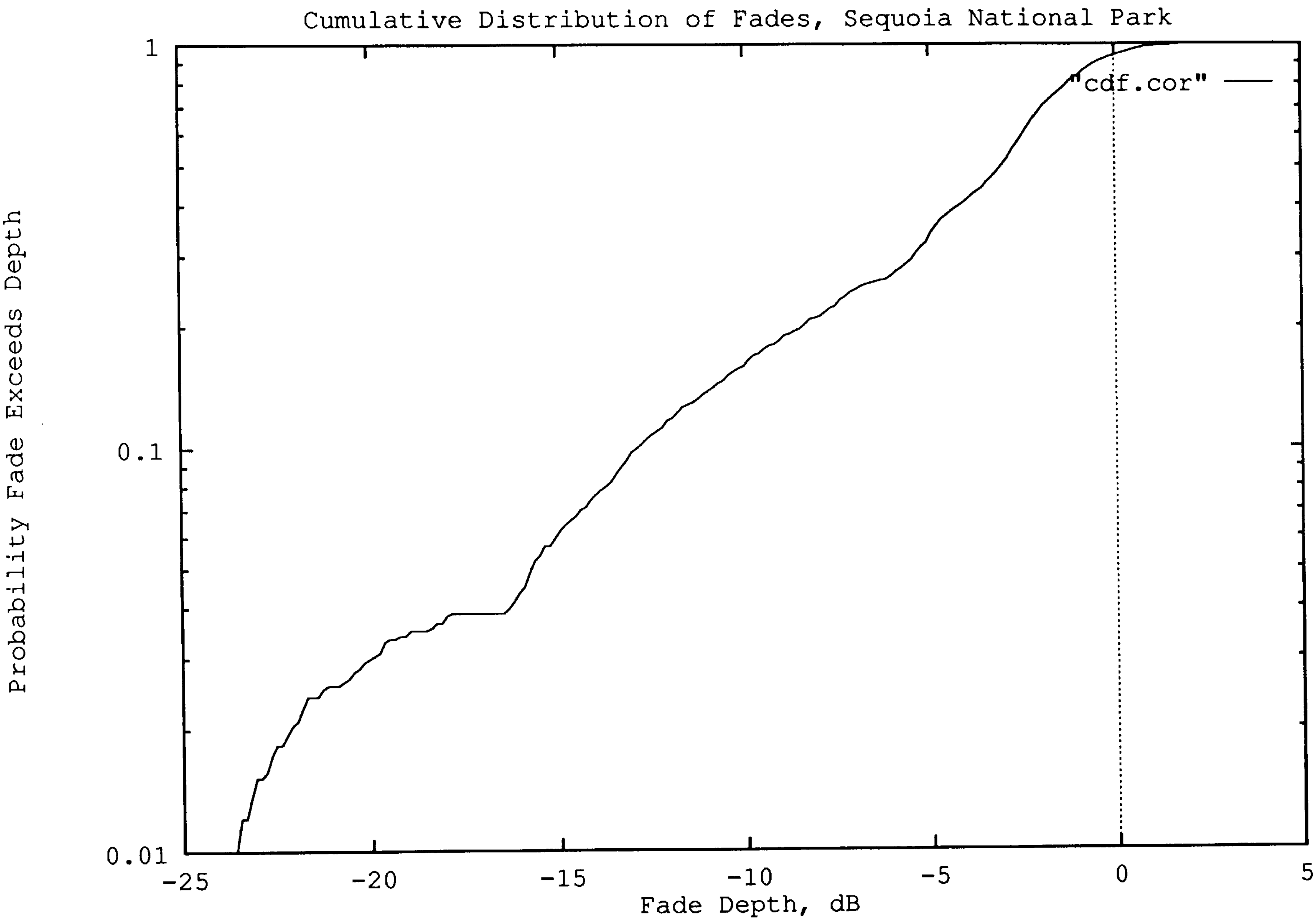
Cumulative Distribution of Fades, Sequoia National Park
"cdf.cor"
Probability Fade Exceeds Depth
1
0.1
0.01
-25
-20
-15
-10
-5
0
5
Fade Depth, dB

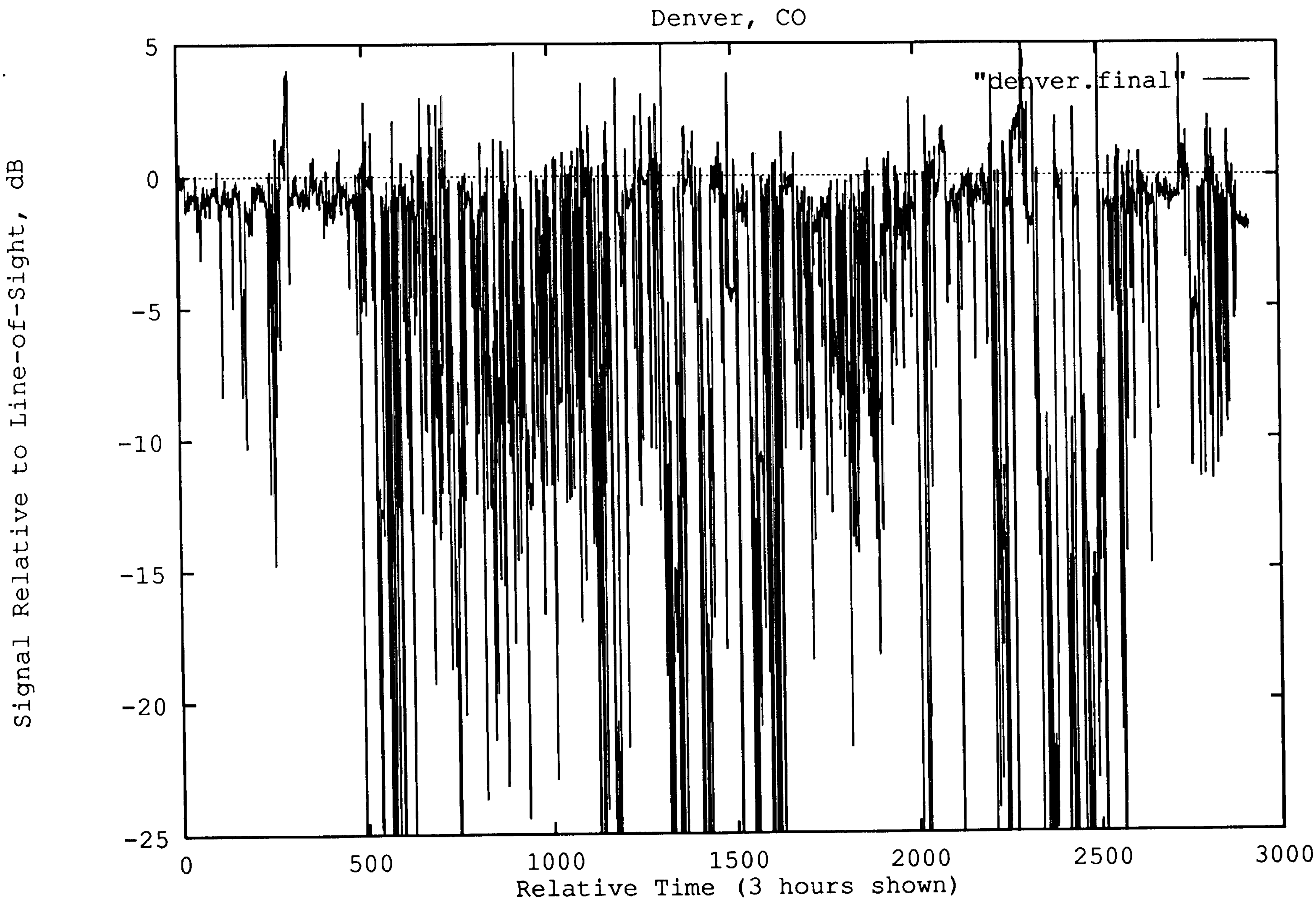

Denver, CO
Signal Relative to Line-of-Sight, dB
5
0
-5
-10
-15
-20
-25
"denver.final"
0
500
1000
1500
2000
2500
3000
Relative Time (3 hours shown)

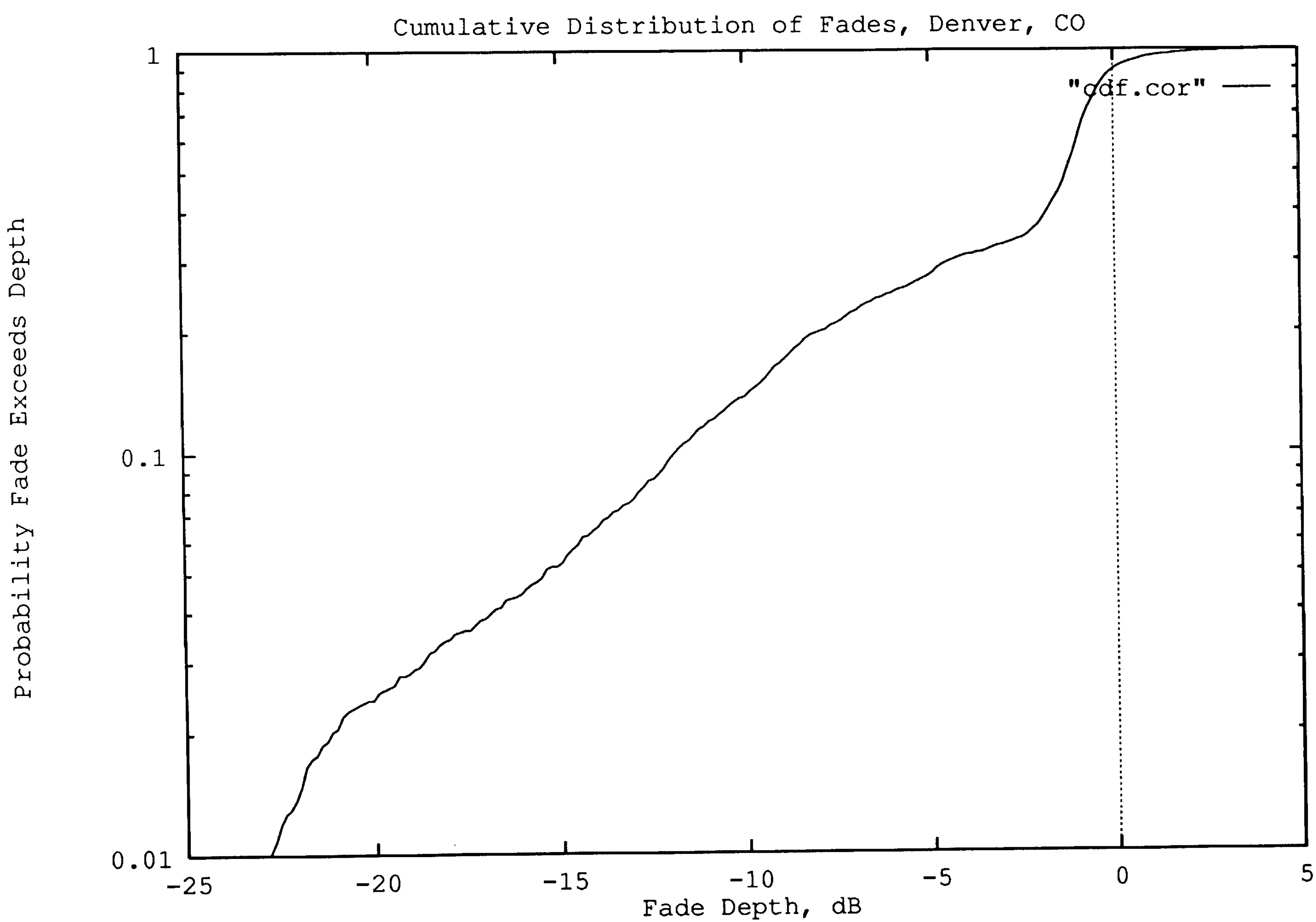

Cumulative Distribution of Fades, Denver, CO
"cdf.cor"
Probability Fade Exceeds Depth
1
0.1
0.01
-25
-20
-15
-10
-5
0
5
Fade Depth, dB

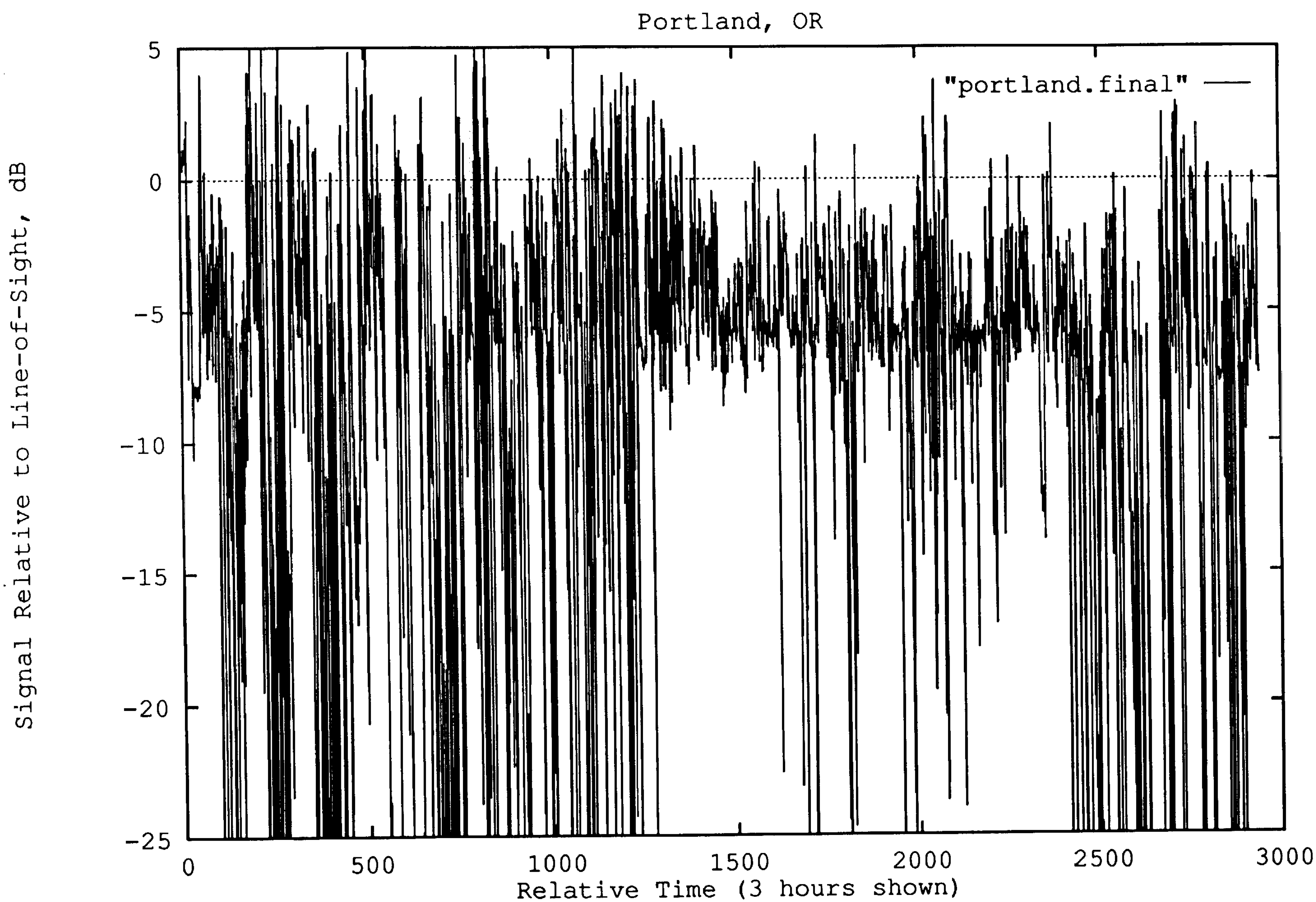

Portland, OR
"portland.final"
Signal Relative to Line-of-Sight, dB
5
0
-5
-10
-15
-20
-25
0
500
1000
1500
2000
2500
3000
Relative Time (3 hours shown)

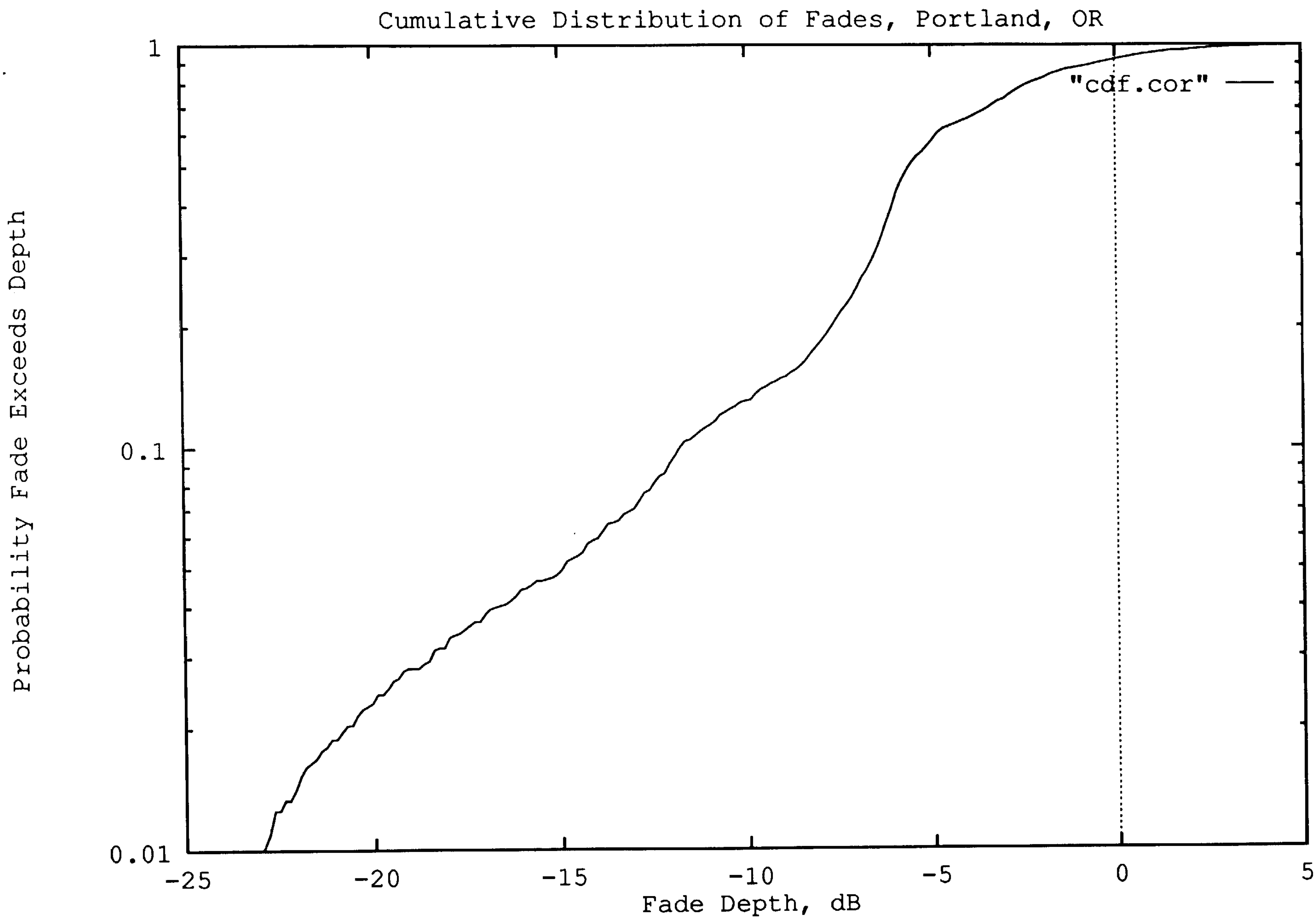
Cumulative Distribution of Fades, Portland, OR
"cdf.cor"
Probability Fade Exceeds Depth
1
0.1
0.01
-25
-20
-15
-10
-5
0
5
Fade Depth, dB

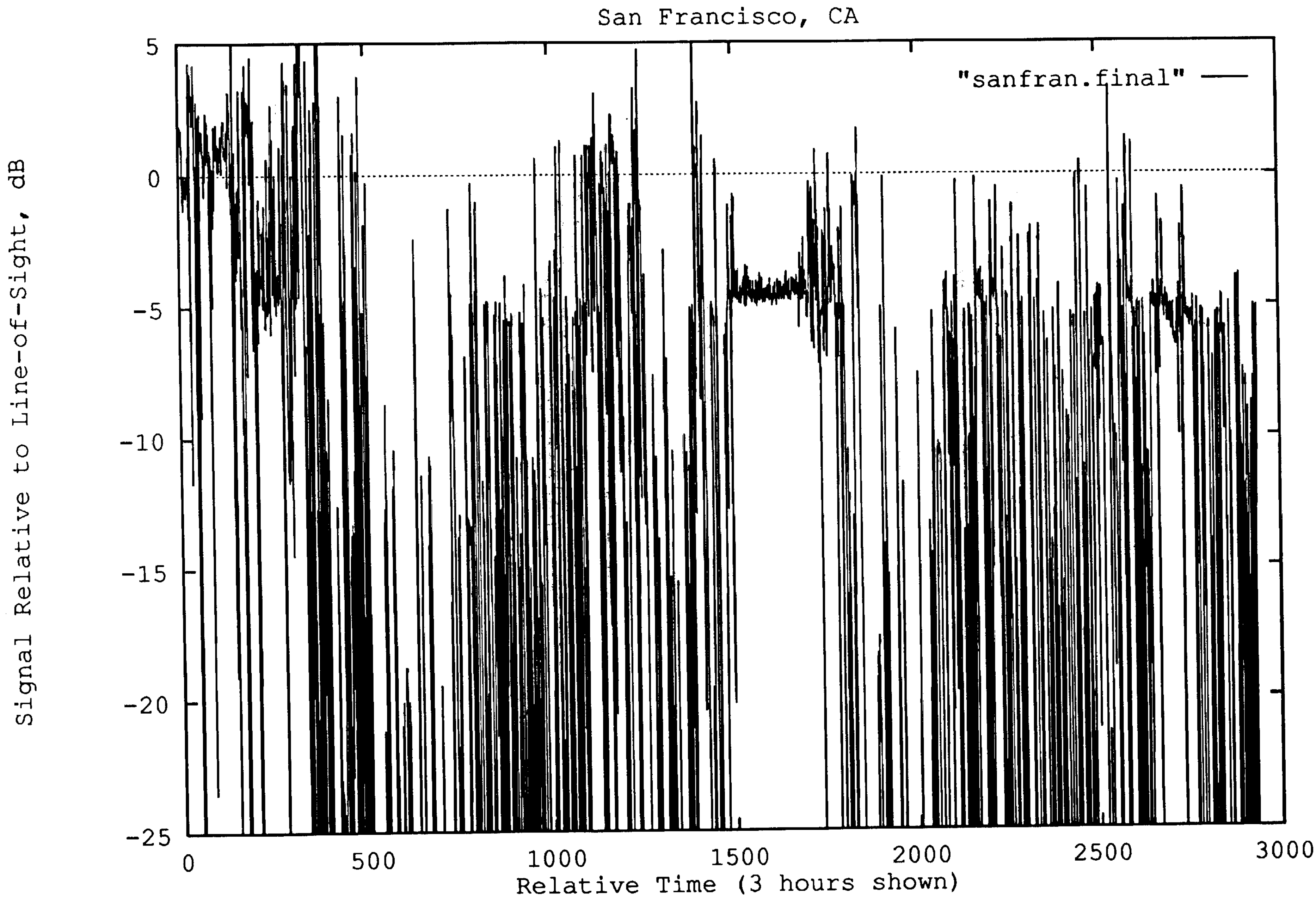

San Francisco, CA
"sanfran.final"
Signal Relative to Line-of-Sight, dB
5
0
-5
-10
-15
-20
-25
0
500
1000
1500
2000
2500
3000
Relative Time (3 hours shown)

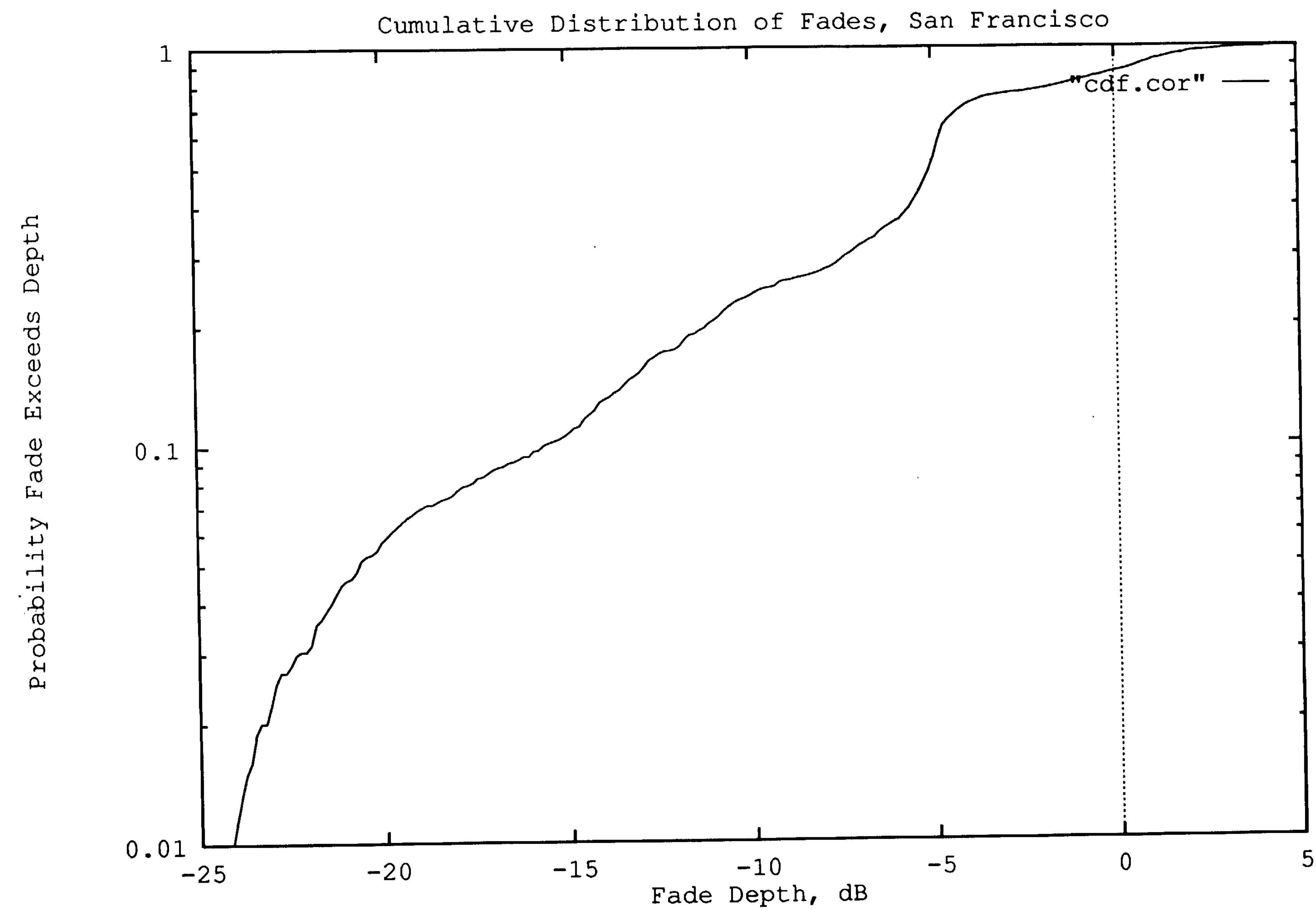
Cumulative Distribution of Fades, San Francisco
Probability Fade Exceeds Depth
1
0.1
0.01
"cdf.cor"
-25
-20
-15
-10
-5
0
5
Fade Depth, dB